Spir-1 promotes IRF3 activation and is targetted by vaccinia virus protein K7

Alice Abreu Torres[1], Stephanie L. Macilwee[¶1], Amir Rashid[1], Sarah E. Cox[1], Jonas D. Albarnaz[1], Claudio A. Bonjardim[2] & Geoffrey L. Smith[1*]

[1]Department of Pathology, University of Cambridge, Tennis Court Road, CB1 2QP, Cambridge, United Kingdom
[2]Laboratório de Vírus, Departamento de Microbiologia, Instituto de Ciências Biológicas, Universidade Federal de Minas Gerais, Belo Horizonte, MG, Brazil.

[¶]Present address: Algal Omega 3, Penrhyn Rd, Knowsley, Prescot L34 9HY

[*]Corresponding author: email, gls37@cam.ac.uk

Running title: Spir-1 is a poxvirus restriction factor

Key words: vaccinia virus, innate immunity, IRF3 activation, interferon, protein K7, virus immune evasion, Spir-1, virus restriction factor

Abstract

Characterisation of viral proteins that mediate immune evasion enables identification of host proteins that function in innate immunity and act as viral restriction factors. This is shown here with vaccinia virus (VACV) protein K7. K7 is a virulence factor that inhibits activation of IRF3 and NF-κB and binds the DEAD-box RNA helicase 3 (DDX3). In this study, Spir-1 is characterised as an additional cellular protein bound by K7 during VACV infection. Spir-1 belongs to a family of actin-binding proteins, however its interaction with K7 does not require its actin-binding domains, suggesting a new function. In human and mouse cells lacking Spir-1, IRF3 activation is impaired, whereas, conversely, Spir-1 overexpression enhanced IRF3 activation. Like DDX3, Spir-1 interacts with K7 directly via a diphenylalanine motif that also is required to promote IRF3 activation. The biological importance of Spir-1 in the response to virus infection is shown by enhanced replication/spreading of VACV in Spir-1 knockout cells. Thus Spir-1 is a new viral restriction factor that functions to enhance IRF3 activation.

Introduction

Successful viral replication requires evasion of host antiviral responses. The host innate immune response to viral infection begins with the sensing of pathogen-associated molecular patterns (PAMPs) by pattern recognition receptors (PRRs), such as Toll-like receptors and retinoic acid-inducible gene-I (RIG-I)-like receptors (RLRs) (Janeway & Medzhitov, 2002; Pang & Iwasaki, 2012). The sensing of virus macromolecules, such as viral DNA or RNA, by PRRs triggers signalling cascades that culminate in the activation of the transcriptional factors interferon regulatory factor (IRF) 3, activator protein (AP) 1 and nuclear factor kappa B (NF-κB) (Thompson *et al*, 2011). These transcriptional factors translocate to the nucleus where they induce the transcription of genes encoding interferons (IFN), cytokines and chemokines. Once secreted from the cell, IFNs bind to their receptors on the surface of infected or non-infected cells, and trigger signal transduction via the JAK-STAT pathway leading to expression of interferon-stimulated genes (ISGs) that induce an antiviral state (Randall & Goodbourn, 2008). During the co-evolution with their hosts, viruses have evolved strategies to evade, suppress or exploit the host response to infection by targetting multiple steps of the host immune response (Garcia-Sastre, 2017).

Vaccinia virus (VACV), the prototypical orthopoxvirus, is well known as the live vaccine used to eradicate smallpox (Fenner *et al*, 1988). VACV has a large dsDNA genome of approximately 190 kbp (Goebel *et al*, 1990), replicates in the cytoplasm (Moss, 2013) and encodes scores of proteins that antagonise innate immunity (Smith *et al*, 2013). Interestingly, some cellular pathways, such as those leading to activation of IRF3 or NF-κB or the JAK-STAT pathway downstream of IFNs binding to their receptors, are targetted by multiple different VACV proteins. Moreover, some of these viral

antagonists are multifunctional and target more than one host innate immune pathway (Smith *et al.*, 2013).

VACV protein K7 is one such antagonist of innate immunity. K7 is a small, intracellular protein that is non-essential for virus replication in cell culture, yet contributes to virulence in both intradermal and intranasal mouse models of infection (Benfield *et al*, 2013). Like several VACV virulence factors, K7 has a Bcl-2-like fold, but lacks an open surface groove that is needed for the interaction with cellular pro-apoptotic proteins (Kalverda *et al*, 2009; Oda *et al*, 2009). Functionally, K7 was reported to suppress NF-κB activation by binding to interleukin-1 receptor-associated kinase-like 2 (IRAK2) and tumour necrosis factor (TNF) receptor-associated factor 6 (TRAF6) (Schroder *et al*, 2008). K7 also inhibits IRF3 activation and binds to the DEAD-box RNA helicase 3 (DDX3) (Schroder *et al.*, 2008). Another study reported that K7 affected regulation of histone methylation during VACV infection, by an unknown mechanism (Teferi *et al*, 2017). Two unbiased proteomic searches identified novel cellular binding partners of K7 (Li *et al*, 2017; Pichlmair *et al*, 2012), suggesting that K7 may have additional functions. The identification of cellular proteins targetted by viral proteins has been a useful approach to identify cellular factors that function in the recognition and restriction of virus infections (Lu *et al*, 2019; Soday *et al*, 2019). In this study, we validated and characterised the interaction between K7 and the cellular protein Spir-1 (Pichlmair *et al.*, 2012) and identified a new function for Spir-1 in innate immunity and as a viral restriction factor.

The protein spire homolog 1 (Spir-1, also known as SPIRE1) was first described in the development of oocytes and embryos in *Drosophila* (Manseau & Schupbach, 1989). Spir-1 has actin-binding domains (Wellington *et al*, 1999) through which it nucleates actin filaments, an activity shared with the Arp2/3 complex and the formins (Quinlan *et al*, 2005). Spir-1 is organised in multiple functional domains. The N-terminal region contains the kinase non-catalytic C-lobe domain (KIND), which mediates Spir-1 interaction with other proteins, such as the formins (Pechlivanis *et al*, 2009). Spir-1 and the formins cooperate during actin nucleation (Bosch *et al*, 2007; Montaville *et al*, 2014; Pfender *et al*, 2011; Quinlan, 2013; Quinlan *et al*, 2007; Schuh, 2011; Tittel *et al*, 2015; Vizcarra *et al*, 2011; Zeth *et al*, 2011). The KIND domain is followed by four actin-binding Wiskott-Andrich syndrome protein homology domain 2 (WH2) domains that are responsible for actin nucleation (Ducka *et al*, 2010; Quinlan *et al.*, 2005; Sitar *et al*, 2011). The C-terminal region of Spir-1 contains a globular tail domain-binding motif (GTBM), which is responsible for binding to myosin V (Pylypenko *et al*, 2016). Next, there is a Spir-box (SB) domain that is conserved within the Spir protein family. Due to its similarity to a helical region of the rabphilin-3A protein that interacts with the GTPase Rab3A, it is thought that the Spir-box domain is involved in the association of Spir-1 and Rab-GTPases. Indeed, Spir-1 co-localises or interacts with several Rab-GTPases (Alzahofi *et al*, 2020; Kerkhoff *et al*, 2001; Lagal *et al*, 2014; Schuh, 2011). Following the SB domain, there is a modified FYVE zinc finger

domain that interacts with negatively-charged lipids in membranes. The membrane targetting specificity is mediated via the interaction of Spir-1 with other membrane-bound proteins such as the Rab-GTPases (Tittel *et al.*, 2015).

Mammals encode two *Spire* genes, *Spire1* and *Spire2* that share high amino acid sequence identity, especially within the WH2 and Spir-box domains (Kerkhoff, 2006; Pleiser *et al*, 2010). The Uniprot database for human Spir-1 (Q08AE8) describes five Spir-1 isoforms produced by alternative splicing and splicing before the GTBM (Exon 9) and SB (Exon 13) domains has been demonstrated (Kollmar *et al*, 2020). The function of isoform 1, which has alternative splicing of exon 9, is unknown, but Spire-1C, which is formed by alternative splicing of exon 13, directs Spir-1 to mitochondria (Kollmar *et al.*, 2020; Manor *et al*, 2015). In adult mice, Spir-1 is expressed preferentially in neuronal and hematopoietic cells (Pleiser *et al.*, 2010; Schumacher *et al*, 2004). Among Spir-1 isoforms, Spir-1 (also known as isoform 2) is the most abundant form in the brain and small intestine tissues (Kollmar *et al.*, 2020) and is the form studied here.

In general, Spir-1 is involved in several actin-dependent cellular functions such as vesicle trafficking (Kerkhoff *et al.*, 2001; Lagal *et al.*, 2014; Morel *et al*, 2009; Schuh, 2011), DNA repair (Belin *et al*, 2015), mitochondrial division (Manor *et al.*, 2015), and development of germ cells (Manseau & Schupbach, 1989; Pfender *et al.*, 2011; Wen *et al*, 2018) but a role in innate immunity has not been described. Interestingly, a genome-wide association study found that a single nucleotide polymorphism in Spir-1 correlated with a different antibody response to smallpox vaccination (Ovsyannikova *et al*, 2012).

Here, Spir-1 is shown to promote IRF3 activation via a diphenylalanine motif that is also necessary for its interaction with VACV virulence factor K7. Using gain of function and loss of function cell lines, Spir-1 is shown to diminish VACV replication and/or spread and is therefore a viral restriction factor.

Results

Vaccinia virus protein K7 co-precipitates with the C terminal region of Spir-1

A previous proteomic study identified Spir-1 as a cellular interacting partner of VACV protein K7 although this interaction was not validated (Pichlmair *et al.*, 2012). To confirm if K7 co-precipitates with Spir-1, HEK293T cells were transfected with plasmids encoding Myc-tagged human Spir-1, Spir-2 or β-TrCP, or Myc-GFP, together with plasmids expressing FLAG-tagged, codon-optimised K7 or another Bcl-2-like VACV protein, A49 (Neidel *et al*, 2015). Immunoprecipitation with anti-Myc or anti-

FLAG affinity resins showed that K7 was co-precipitated by Myc-Spir-1 (Fig. 1A), but not by Myc-Spir-2, Myc-β-TrCP or Myc-GFP. In contrast, A49 interacted with β-TrCP as reported (Mansur *et al*, 2013), but not with the other proteins. Reciprocally, FLAG-K7 co-precipitated Spir-1 (Fig. 1B), but not the other Myc-tagged proteins, whilst β-TrCP only interacted with A49.

To investigate if the actin-binding domains of Spir-1 were needed for interaction with K7, two Myc-tagged truncations of Spir-1 were generated: an N-terminal region (amino acid residues 1-390), containing the four actin-binding WH2 domains and the KIND domain; and a C-terminal region, containing the Spir-box and FYVE domains (amino acid residues 391-742, Fig. 1C). These truncations, Spir-1 or Spir-2, were co-expressed with FLAG-K7 and Myc-tagged immunoprecipitation showed that the C terminus of Spir-1 was sufficient for interaction with K7, whereas the actin-binding domains were dispensable (Fig. 1D, middle panel). The reciprocal IP gave the same conclusion and FLAG-K7 co-precipitated full-length Spir-1 and its C-terminal region (Fig. 1D, right panel). As controls, the N-terminal region co-precipitated endogenous actin via its WH2 domains, and the C-terminal region interacted with 14-3-3, another binding partner of Spir-1 (Benzinger *et al*, 2005; Ewing *et al*, 2007).

To determine if Spir-1 and K7 interacted at endogenous levels, cells were either mock-infected or infected with VACV expressing HA-tagged K7 (vHA-K7) (Benfield *et al.*, 2013) or B14 (vHA-B14) (Chen *et al*, 2006). HA-immunoprecipitation confirmed that K7 interacts with endogenous Spir-1, whilst B14 does not (Fig. 1E). As reported, K7 also co-precipitated with DDX3 (Schroder *et al.*, 2008), and B14 interacted with IKKβ (Chen *et al*, 2008). Altogether, these results indicate that Spir-1, but not Spir-2, interacts with K7 via its C-terminal region and independent of its actin-binding domains.

Ectopic Spir-1 increases IRF3-dependent gene expression

Since the interaction of Spir-1 with K7 is independent of binding actin, and K7 is a VACV immunomodulator and virulence factor, we hypothesised that Spir-1 might have a hitherto unknown function in antiviral immunity. To test this, the impact of Spir-1 on innate immune signalling pathways was assessed by luciferase reporter gene assays. First, cells were transfected with a reporter plasmid in which the expression of firefly luciferase is driven by the IFNβ promoter. IFNβ expression was induced by Sendai virus (SeV) infection, which is sensed by RIG-I leading to IRF3 activation (Pichlmair *et al.*, 2012). Myc-Spir-1 expression alone did not affect IRF3 activation, however, Spir-1 augmented activation induced by SeV infection (Fig. 2A). In contrast, Myc-tagged GFP had no effect, and VACV protein C6 was inhibitory, as described (Unterholzner *et al*, 2011). Spir-1 did not affect activation of ISRE-dependent gene expression downstream of type I IFN, whereas C6, but not N1, was inhibitory (Stuart *et al*, 2016) (Fig. 2B). Similarly, Spir-1 did not affect NF-κB activation in response

to TNF-α, whilst B14 inhibited it (Chen *et al.*, 2008) and VACV protein N2 had no effect (Ferguson *et al*, 2013) (Fig. 2C). Further analysis using an IRF3-specific reporter plasmid (ISG56.1 or IFIT1 promoter) showed Spir-1 caused a dose-dependent increase in IRF3 activation induced by the CARD domain of RIG-I (Fig. 2D, E). As controls, VACV protein N2 inhibited IRF3 activation as described (Ferguson *et al.*, 2013) while A49, an NF-κB inhibitor (Mansur *et al.*, 2013), did not. Unlike Spir-1, Spir-2 did not enhance IRF3 activation whereas DDX3 did, as described (Schroder *et al.*, 2008) (Fig. 2E).

To map at which stage in the IRF3 pathway Spir-1 was acting, further ISG56.1 reporter assays were performed in which the pathway was stimulated by expression of its different components. Spir-1 activated the IRF3 pathway in a dose-response manner when MAVS (mitochondrial antiviral-signalling protein) was used as stimulant (Fig. 2F), but not when downstream components such as TBK1 (Fig. 2G), IKKε (Fig. EV1) or the constitutively active IRF3-5D (Fig. 2H) were expressed. These findings indicate Spir-1 enhances IRF3 activation at or downstream of MAVS and upstream of IKKε or TBK1. Finally, N- and C-terminal fragments of Spir-1 were tested following stimulation by RIG-I CARD. Neither half of Spir-1 activated the pathway fully, but the C-terminal region had greater activity than the N-terminal region (Fig. 2I).

Spir-1 interaction with K7 is independent of DDX3, direct and via a diphenylalanine motif

K7 interacts directly with DDX3 (Kalverda *et al.*, 2009; Oda *et al.*, 2009), an adaptor protein in the IRF3 pathway (Fullam & Schroder, 2013; Gu *et al*, 2017). To investigate whether K7 binding to Spir-1 was via DDX3, cells stably expressing an inducible shRNA targetting DDX3 (shDDX3) (Gu *et al.*, 2017) were used. Knockdown, rather than knockout, of DDX3 was utilised because *DDX3* encodes an essential protein (Wang *et al*, 2015). Cells expressing a non-silencing control (NSC) shRNA were used in parallel. DDX3 knockdown was induced by incubation with doxycycline (DOX) for 48 h as described (Gu *et al.*, 2017), prior to transfection with either FLAG-tagged K7 or A49 for 24 h. Viral proteins were immunoprecipitated via their FLAG tag, followed by immunoblotting for endogenous Spir-1. DDX3 levels were reduced greatly in shDDX3 cells following DOX treatment, but not in control cells (Fig. 3A). Despite this, Spir-1 co-precipitation by K7 was unaffected (Fig. 3A). A49 did not co-precipitate either DDX3 or Spir-1 (Fig. 3A). Next, the shDDX3 cells were used to determine if DDX3 contributed to Spir-1-induced IRF3 activation. After DDX3 knockdown, there was no significant difference in IRF3 stimulation by Spir-1 (Fig. 3B). Notably, K7 inhibited IRF3 activation when DDX3 was knocked down, showing K7 had another IRF3 inhibitory mechanism independent of DDX3 (Fig. 3B). Moreover, the presence of K7 reversed the activation of the pathway by Spir-1 (Fig. 3B). In summary, Spir-1 interaction with K7 and its function in the IRF3 pathway are independent of DDX3.

Since both DDX3 and Spir-1 bind to K7 and activate IRF3, their amino acid sequences were compared. The structure of K7 bound to a DDX3 peptide and subsequent structure-based mutagenesis, showed a diphenylalanine (FF) motif in DDX3 is essential for binding K7 and for IRF3 activation (Oda *et al.*, 2009). An alignment of the C terminus of Spir-1 and the minimal ten-amino acid peptide from DDX3 (residues 81-90) needed for binding K7, showed a similar FF motif in Spir-1 (Fig. 3C). To determine if this was important for Spir-1 binding to K7, the phenylalanines were mutated to alanines (FFAA) and the mutant was expressed in cells together with FLAG-tagged K7. Wild-type (WT) Myc-Spir-1 and Myc-GFP were also expressed. Anti-Myc or anti-FLAG immunoprecipitation showed that the FFAA mutation impaired Spir-1 interaction with K7 (Fig. 3D), although it still precipitated both actin and 14-3-3, indicating normal folding. Notably, the FFAA mutant no longer activated IRF3 (Fig. 3E).

To determine if the K7 interaction with Spir-1 was direct, these proteins were expressed by *in vitro* transcription and translation and immunoprecipitated alongside Myc-tagged TAB2 and FLAG-tagged VACV protein F12 (Carpentier *et al*, 2015) as controls. Both Spir-1 and DDX3 interacted directly with K7, whereas Spir-1 did not interact with F12, and K7 did not interact with TAB2 (Figs. 3F, 3G). Taken together, this demonstrated that Spir-1 binds directly to K7 and shares with DDX3 a conserved diphenylalanine motif, which is required for its function in the IRF3 pathway.

K7 uses the same amino acid residues to target both Spir-1 and DDX3

K7 binds to the DDX3 peptide through a hydrophobic pocket within a negatively-charged face (Kalverda *et al.*, 2009; Oda *et al.*, 2009). Thus, interactions between K7 and the DDX3 peptide involve hydrophobic contacts, hydrogen bonds and electrostatic interactions, of which electrostatic contacts between R88 of DDX3 with both D28 and D31 of K7 are notable. R31 also forms a hydrogen bond with DDX3 S83 (Oda *et al.*, 2009). Using this information, K7 mutants were generated in an attempt to distinguish between K7 binding to Spir-1 and DDX3. D28 and D31 were changed singly or together to alanine (D28A, D31A) and expressed alongside WT K7 or GFP, and together with Myc-tagged Spir-1 and HA-tagged DDX3. Immunoprecipitation showed that K7 D28A still bound both Spir-1 and DDX3, whilst K7 D31A had impaired binding to both proteins, especially DDX3 (Fig. 4A). Furthermore, the double mutant (DDAA) had further reduced binding to Spir-1 and no detectable binding to DDX3 (Fig. 4A). Importantly, all mutants still interacted with COPε (Fig. 4A), another K7 binding partner (Li *et al.*, 2017), suggesting normal K7 folding. Co-precipitation of endogenous Spir-1 with FLAG-tagged K7 and mutants gave similar conclusions (Fig. 4B). Notably, the K7 D31A mutant inhibited IRF3 activation poorly compared to the WT or D28A (Fig. 4C). Altogether, these data indicate that K7 requires D31 for interacting with both DDX3 and Spir-1 and via each interaction it inhibits the IRF3

pathway.

IRF3 activation is reduced in the absence of Spir-1

To investigate Spir-1-mediated activation of IRF3 further, Spir-1 knockout (KO) cell lines were generated by CRISPR-Cas9-mediated targetting of *Spire1* exon 3, which is conserved in all Spir-1 isoforms (Fig. 5A). After single cell selection, HEK293T cell lines were confirmed to lack Spir-1 by immunoblotting (Fig. 5B) and by sequencing of both *Spire-1* alleles (Fig. 5A). A clone that lacked Spir-1 and in which the *Spire-1* open reading frame was disrupted by frameshift mutations in both alleles and that lacked WT sequence, was selected. Additionally, a vector expressing Myc-tagged Spir-1 were used to rescue Spir-1 expression in the KO cell line following lentiviral transduction. In parallel, both WT and KO cells were transduced with a control empty vector (EV) lentivirus. Spir-1 WT cells transduced with EV, and Spir-1 KO cells transduced with EV or Myc-Spir-1 were infected with SeV to activate the IRF3 pathway. Supernatants were collected for ELISA and cells lysates were used for either RNA extraction or immunoblotting, which confirmed that cells did or did not express Spir-1 (Fig. 5B). The expression of Myc-Spir-1 increased in the presence of SeV, but this was not observed for endogenous Spir-1 (Fig. 5B). One possible explanation is that Myc-Spir-1 expression is driven by the human cytomegalovirus immediate early promoter (Everett *et al*, 2009) that contains binding sites for transcription factors such as NF-κB (Stinski & Meier, 2007), which can also be activated during SeV infection. The phosphorylation of IRF3 at S532 (p-IRF3) increased greatly 24 h after SeV infection of WT cells (Fig. 5B) but was reduced in the absence of Spir-1 and restored in the KO cells expressing Myc-Spir-1 (Fig. 5B). Moreover, after SEV infection, Spir-1 KO cells produced lower levels of mRNAs for *ISG56/IFIT1* (Fig. 5C), *IFNB1* (Fig. 5D) and *CXCL10* (Fig. 5E) and secreted less CXCL-10 (Fig. 5F) as measured by RT-qPCR and ELISA, respectively. Importantly, the absence of Spir-1 did not change the levels of CXCL-10 secreted in response to TNF-α, a specific agonist of the NF-κB pathway (Fig. 5G).

Immortalised mouse embryonic fibroblasts (MEFs) from mice with a terminator (gene trap) between exons 3 and 4 of the *Spire1* gene (Pleiser *et al*, 2014) were used to investigate the contribution of Spir-1 to IRF3 activation in cells from a different mammal. After stimulation of IRF3 by either poly I:C or SeV infection, MEFs were lysed for immunoblotting or RNA analysis and supernatants were collected for ELISA. A reduction in p-IRF3 was seen in Spir-1 KO cells (Fig. 6A, B) and this was quantified by normalisation to α-tubulin (bottom graphs in Figs 6A, B). The Spir-1 KO MEFs also expressed less mRNAs for cytokines and chemokines upon stimulation with poly I:C or SeV infection than their WT controls (Figs. 6C-H). Likewise, CXCL-10 and IL-6 secretion were lower from Spir-1 KO cells (Figs. 6I-L). However, the levels of CXCL-10 and IL-6 secreted after stimulation with IL-1β

were not reduced in Spir-1 KO MEFs (Fig. 6M, N); indeed there was a small increase in IL-6 levels in KO cells (Fig. 6N). In summary, in both mouse and human cells there is a defect in IRF3 activation downstream of RIG-I/MDA5, whilst other immune signalling pathways were largely unaltered.

Spir-1 is a restriction factor for VACV

Given that Spir-1 interacts with VACV protein K7 and enhances IRF3 activation, which is critical for the host response to viral infection, the impact of Spir-1 on VACV replication and spread was assessed. Spir-1 WT and KO HEK293T cells and the derivative cell line in which Spir-1 expression was restored in the KO cells, were infected with A5-GFP-VACV, a VACV strain expressing GFP fused to capsid protein A5 (Carter *et al*, 2003), and 2 days (d) later plaque diameters were measured (Fig. 7A, B). A significant increase in plaque size was seen in the absence of Spir-1 compared to both WT and rescued cells (Fig. 7B), suggesting that Spir-1 restricts VACV spread and/or replication. Lastly, virus growth on those cells was assessed. Cells were infected with 0.001 plaque-forming unit/cell of VACV strain WR and 2 d later the virus yield was determined by plaque assay. Spir-1 KO cells yielded higher viral titres compared to both WT and Spir-1 complemented cells (Fig. 7C). Collectively, loss of Spir-1 caused an increase in both virus plaque size and yield of infectious virus, showing that Spir-1 functions as a restriction factor against VACV.

Discussion

During co-evolution with their hosts, viruses have evolved mechanisms to evade the host antiviral responses and thereby replicate and spread efficiently. Such virus proteins are numerous and have diverse functions and, therefore, can be used to gain insight into how the host innate immune system functions. VACV is a poxvirus and encodes scores of immunomodulatory proteins many of which target the innate immune system. In several cases, multiple VACV proteins engage the same pathway, but despite this, these proteins each contributes to virulence indicating non-redundant functions (Smith *et al.*, 2013). Sometimes a single protein can inhibit multiple pathways (Smith *et al.*, 2013) or an open reading frame can encode multiple proteins with different functions (Neidel *et al*, 2020). High-throughput proteomic approaches have been used to identify binding partners of VACV proteins, or cellular proteins that are up or down-regulated during virus infection, and such cellular proteins may have antiviral activity and function in innate immunity (Pichlmair *et al.*, 2012; Soday *et al.*, 2019). For example, histone deacetylases (HDAC) 4 and 5 are each bound by VACV protein C6 and function as a virus restriction factor (Lu *et al.*, 2019; Soday *et al.*, 2019).

Here, Spir-1 is characterised as another cellular protein that is bound by VACV protein K7 (Fig. 1), a

virulence factor that inhibits NF-κB and IRF3 activation (Benfield *et al.*, 2013; Schroder *et al.*, 2008). K7 binding to Spir-1 was identified in a proteomic screen for binding partners of virus immunomodulatory proteins (Pichlmair *et al.*, 2012). Here this interaction is confirmed, demonstrated to occur at endogenous levels during VACV infection (Fig. 1E), and shown to be direct (Fig. 3F, G).

Spir-1 belongs to a family of proteins involved in actin organisation (Kerkhoff, 2006) but K7 interaction with Spir-1 does not require its N-terminal actin-binding domain (Fig. 1D). VACV induces polymerisation of actin to facilitate virus dissemination from the cell surface and VACV mutants unable to polymerise actin spread poorly and form small plaques (Smith *et al*, 2002). However, a mutant lacking K7 produces normal size plaques (Benfield *et al.*, 2013). Given that K7 is an immunomodulatory protein, we hypothesised that Spir-1 might have a function in innate immunity. In reporter gene assays, Spir-1 over-expression enhanced IRF3-dependent gene expression (Fig. 2D),but did not affect JAK-STAT signalling induced by type I IFN, or NF-κB activation (Fig. 2B, C). Conversely, human and murine Spir-1 knockout cell lines showed diminished IRF3 signalling, with reduced IRF3 phosphorylation and reduced transcription and expression of IRF3-responsive genes (Figs. 5B, 6A, B). Importantly, rescue of Spir-1 expression in Spir-1 KO cells restored phospho-IRF3 and cytokine expression levels (Fig. 5).

To map where Spir-1 influences IRF3 activation, the pathway was activated by different agonists and the influence of Spir-1 examined. Spir-1 enhanced activation induced by SeV infection (Fig. 2A, 5 & 6), Poly I:C transfection (Fig. 6), and overexpression of RIG-I CARD (Fig. 2D, E) and MAVS (Fig. 2F), but not overexpression of TBK1, IKKε or a constitutively active IRF3 (Fig. 2G and sup). SeV RNA is sensed by RIG-I (Kato *et al*, 2005) whilst high molecular weight (HMW) poly I:C is sensed by MDA-5 (Kato *et al*, 2008; Kato *et al*, 2006). This suggests Spir-1 acts at or downstream of MAVS, the adaptor molecule recruited downstream of RIG-I and MDA5 activation (Brisse & Ly, 2019). The association of RIG-I/MDA5 with MAVS results in the recruitment of tumour necrosis factor receptor-associated factors (TRAF), such as TRAF3, leading to the phosphorylation of IRF3 by TBK1/IKKε. Collectively, these data suggest Spir-1 functions around the MAVS or TRAF3 level. To seek further mechanistic insight into how Spir-1 influences the IRF3 pathway, unbiased proteomic searches for Spir-1-binding partners were undertaken in HEK293T cells infected with SeV, however, under the condition tested, no protein linked to the IRF3 pathway was detected.

K7 inhibition of IRF3 activation was attributed to direct binding to DDX3, which acts as a multifunctional scaffolding adaptor culminating in IRF3 activation (Fullam & Schroder, 2013; Gu *et al.*, 2017). However, data presented here show K7 has additional targets within the IRF3 pathway, since Spir-1 also contributes to IRF3 activation and K7 is able to inhibit IRF3 activation even in the absence

of DDX3. Furthermore, DDX3 and Spir-1 act at different positions in the pathway; DDX3 acts at the TRAF3 and TBK1/IKKε level (Gu *et al.*, 2017; Schroder *et al.*, 2008; Smith *et al.*, 2013; Soulat *et al*, 2008), whilst Spir-1 acts upstream of TBK1/IKKε (Fig. 2). Interestingly, both DDX3 and Spir-1 share a diphenylalanine motif that is responsible for both binding to K7 and their function in the IRF3 pathway (Fig. 3) (Oda *et al.*, 2009). Furthermore, the same amino acid residue in K7 (D31) is crucial for its binding to both cellular proteins (Fig. 4). This prevents easy assessment of the relative importance of K7 binding to each cellular protein.

Nonetheless, Spir-1 has an important antiviral role because cells lacking Spir-1 show enhanced VACV replication and/or spread (Fig. 7). Comparable data for DDX3 are lacking, and obtaining such data is complicated by DDX3 being an essential protein. Both K7 and Spir-1 localise in the cytoplasm (Benfield *et al.*, 2013; Kerkhoff *et al.*, 2001). Interestingly, mutations in the FYVE domain and in the diphenylalanine motif in Spir-1 affect its sub-cellular localisation, changing from a trans-Golgi network and post-Golgi vesicles localisation to an even cytoplasmic distribution (Kerkhoff *et al.*, 2001; Tittel *et al.*, 2015). Neither the N- or C-terminal halves of Spir-1 were capable of activating the IRF3 pathway as well as full-length protein (Fig. 2I), despite comparable expression levels, suggesting that both halves are important. Possibly, Spir-1 is targetted to the correct location by its C-terminal domain, whist its N-terminal domain mediates Spir-1 engagement with other proteins to promote IRF3 activation. This might explain why the FFAA Spir-1 mutant is no longer able to activate the IRF3 pathway. Another possibility is that K7 may bind to the Spir-1 diphenylalanine motif and displace other proteins or sequester it and prevent it reaching its subcellular location. Spir-1 has several isoforms (Kollmar *et al.*, 2020), and one, Spire-1C (also known as Spire1-E13), differs from the canonical isoform by encoding an extra exon sequence (ExonC or E13), which mediates its mitochondrial localisation and regulates mitochondrial division (Manor *et al.*, 2015). Even though this was not the isoform used in the present study, K7 might regulate Spir-1 trafficking to the mitochondrion, where MAVS is anchored (Seth *et al*, 2005). In the future, it would be interesting to check the cellular localisation of Spir-1 upon IRF3 activation and whether K7 could alter this localisation.

RIG-I and MDA5 can sense RNA virus genomes directly, but also RNA generated by infection with DNA viruses (Weber *et al*, 2006), leading to IRF3 activation. Therefore, RIG-I/MDA5-triggered antiviral response is antagonised by several RNA and DNA viruses (Brisse & Ly, 2019; Liu *et al*, 2016). It has long been known that dsRNA is generated during VACV infection (Colby & Duesberg, 1969; Pichlmair *et al*, 2009; Rice *et al*, 1984), so it is not surprising that VACV encodes proteins to interfere with cytosolic RNA sensing. For instance, VACV protein E3 binds to dsRNA and prevents RIG-I-dependent sensing of RNA products generated via the transcription of AT-rich DNA by RNA polymerase III (Marq *et al*, 2009);(Valentine & Smith, 2010), and the decapping enzymes D9 and D10 prevent the

accumulation of dsRNA from viral complementary RNA molecules (Liu *et al*, 2015). Downstream of RNA sensing, VACV encodes proteins to inhibit IRF3 activation, such as C6, which acts at TBK1/IKKε activation level (Unterholzner *et al.*, 2011), N2, which acts downstream of IRF3 translocation to the nucleus (Ferguson *et al.*, 2013) and K7, which targets DDX3 (Schroder *et al.*, 2008). Here we show that Spir-1 also contributes to IRF3 activation, with both Spir-1 and DDX3 sharing a similar motif targetted by K7.

In summary, Spir-1 is another cellular protein that affects IRF3 activation and is a virus restriction factor. By exploring in detail VACV protein K7 function, a new cellular factor that regulates IRF3 activation and acts as a viral restriction factor has been characterised.

Material and Methods

Cells lines

Human embryonic kidney (HEK) 293T, HEK293T NSC or shDDX3 (kind gifts from Dr. Martina Schröder, Maynooth University, Ireland), murine embryonic fibroblasts (MEFs) Spir-1 KO and WT (kindly provided by Prof. Dr. Eugen Kerkhoff - University Hospital Regensburg, Germany) and BSC-1 (African Green Monkey) cells were cultured in Dulbecco's modified Eagle's medium (DMEM, Gibco) supplemented with 10% heat-treated (56 ºC, 1 h) foetal bovine serum (FBS, Pan Biotech), 100 U/ml penicillin and 100 µg/ml streptomycin (P/S, Gibco). RK13 cells were grown in minimal essential medium (MEM, Gibco) supplemented with 10% FBS and P/S.

Viruses

VACV strain Western Reserve (WR) and derivative strains expressing GFP fused to the capsid protein A5 (A5-GFP-VACV) (Carter *et al.*, 2003), VACV expressing HA-tagged B14 (Chen *et al.*, 2006) and VACV expressing HA-tagged K7 (Benfield *et al.*, 2013) were described. VACV strains were grown on RK13 cells and titrated by plaque assay on BSC-1 cells. Sendai virus (SeV) Cantell strain (Licence No. ITIMP17.0612A) was a gift from Steve Goodbourn (St George's Hospital Medical School, University of London).

Plasmids

A plasmid encoding the Myc-tagged human Spir-1 isoform 2 and human Spir-2 (Pechlivanis *et al.*, 2009) constructs were a kind gift of Prof. Dr. Eugen Kerkhoff. Spir-1 N- and C-terminal truncations were constructed by PCR amplification from pcDNA3.1-Myc-Spir-1 and inserted into plasmid pcDNA3.1-Myc. Codon-optimised FLAG-K7 was described (Torres *et al*, 2016) and Spir-1 and K7 plasmids were used as templates for site-directed mutagenesis according to the instructions of the

QuikChange Site-Directed Mutagenesis Kit (Agilent). All mutations were confirmed by DNA sequencing. Myc-DDX3 and HA-DDX3 (Schroder *et al.*, 2008) were kindly provided by Dr. Martina Schröder. The IFNβ-firefly luciferase reporter plasmid was from T. Taniguchi (University of Tokyo, Japan), NF-κB-firefly luciferase was from R. Hofmeister (University of Regensburg, Germany) and ISG56.1-firefly luciferase was a gift from Ganes Sen (Cleveland Clinic, USA). ISRE-firefly luciferase and pTK-renilla luciferase (pRL-TK) plasmids were from Promega. Vectors expressing MAVS, IKKε, TBK1 and IRF3-5D (Unterholzner *et al.*, 2011) RIG-I-CARD domain (Odon *et al*, 2018) were described. Lentivirus vector plasmid pLKO.DCMV.TetO.mcs (pLDT) (Everett *et al*, 2013) was a gift from Roger Everett (University of Glasgow, UK) and was used as backbone for sub-cloning the Myc-Spir-1. Plasmids pCMV.dR8.91 (expressing all necessary lentivirus helper functions) and pMD-G (expressing the vesicular stomatitis virus envelope protein G) were from Heike Laman (University of Cambridge, UK). pF3A WG plasmid was from Promega. px459 CRISPR-Cas9 plasmid was purchased from Addgene. More information about plasmids and oligonucleotide primers used are given in the reagents table.

Antibodies and Reagents

Primary antibodies used were from the following sources: rabbit (Rb) anti-Myc (Cell Signaling, 2278), mouse (Ms) anti-Myc (Cell Signaling, 9B11), Rb anti-Actin (Sigma, A2066), Ms anti-FLAG (Sigma F1804), Rb anti-14-3-3 (Santa Cruz, sc-629), Ms anti -Spir-1 (Santa Cruz, sc-517039), Ms anti- Spir-1 (Abcam, ab57463), Rb anti-DDX3 (Cell Signaling, 2635), Rb anti-IKKβ (Cell Signaling, 2684), Rb anti-HA (Sigma, H6908), Ms anti-α-Tubulin (Millipore, 05-829), Ms anti-GAPDH (Sigma, G8795), Rb anti-IRF3 (Cell Signaling, 4962), Ms anti-COPε (Santa Cruz, sc-133194), Rb anti-phospho-IRF3 Ser396 (Cell Signaling, 4947S) and Rb polyclonal anti-C6 (Unterholzner *et al.*, 2011). For dilutions used for the primary antibodies, see reagents table. Secondary antibodies used (1:10,000 dilution) were IRDye 680RD-conjugated goat anti-rabbit IgG or anti-mouse IgG and IRDye 800CW-conjugated goat anti-rabbit IgG or anti-mouse IgG (LI-COR).

Reagents used in this study were: Anti-c-Myc Agarose from Santa Cruz Biotechnology, and monoclonal Anti-HA-Agarose, clone HA-7, ANTI-FLAG M2 Affinity Gel and Poly-D-lysine hydrobromide (all from Sigma Aldrich). Human IFNα, human TNF-α and mouse IL-1β were from Peprotech, HMW poly(I:C) and puromycin were from InvivoGen and doxycycline was from Melford.

Reporter Gene Assay

HEK293T cells were seeded in 96-well plates with 1.5×10^4 cells per well. After two days, cells were transfected with 60 ng per well of the firefly luciferase reporter plasmids (IFNβ, ISRE, NF-κB or ISG56.1), 10 ng per well of pTK-renilla luciferase and different amounts of the expression plasmid

under test or empty vector (EV) control using polyethylenimine (PEI, CellnTec, 2 µL per 1 µg DNA). When necessary, EV plasmid was added to the transfection so that the final amount of DNA transfected was kept constant. In cases where stimulation was done by transfecting another plasmid, the same amount of EV was transfected to the non-stimulated (NS) control wells. Cells were stimulated as shown in the Figs: (i) infection with SeV for 24 h (IFNβ Luc), (ii) 10 ng/mL of TNF-α for 8 h (NF-κB Luc) or (iii) with 1000 U/ml of IFNα for 8 h (ISRE-Luc). After stimulation, cells were washed with PBS, lysed with 100 uL/well of passive lysis buffer (Promega) and firefly and renilla luciferase activities were measured using a FLUOstar luminometer (BMG). The firefly luciferase activity in each sample was normalised to the renilla luciferase activity and fold inductions were calculated relative to the non-stimulated controls for each plasmid. In all cases, data shown are representative from at least three independent experiments with at least triplicate samples analysed for each condition.

Immunoblotting

HEK293T (8 x 10^5) or MEFs (2 × 10^5) cells were seeded in 6-well plates and 24 h later cells were stimulated by infection with SeV or transfection with 5 µg/mL of poly I:C using lipofectamine 2000 (Life Technologies). After stimulation, cells were washed twice with ice-cold PBS, and scrapped into a cell lysis buffer containing 50 mM Tris-HCl pH 8, 150 mM NaCl, 1 mM EDTA, 10% (v/v) glycerol, 1% (v/v) Triton X-100 and 0.05% (v/v) NP-40, supplemented with protease (cOmplete Mini, Roche) and phosphatase inhibitors (PhosSTOP, Roche). Protein concentration was determined using a bicinchoninic acid protein assay kit (Pierce) before being boiled at 100 ºC for 5 min. Proteins were then separated by SDS-polyacrylamide gel electrophoresis and transferred onto a nitrocellulose Amersham Protran membrane (GE Healthcare). Membranes were blocked at room temperature with either 5% (w/v) milk or 5% (w/v) bovine serum albumin (BSA, Sigma) in PBS containing 0.1% Tween 20. Then, membranes were incubated with a specific primary antibody diluted in blocking buffer at 4 ºC overnight. After washing, membranes were probed with LI-COR secondary antibodies at room temperature followed by imaging using the LI-COR Odyssey imaging system, according to the manufacturer's instructions. Where indicated, protein bands from three independent experiments were quantified by using Odyssey software (LI-COR Biosciences).

Immunoprecipitation

HEK293T cells were seeded in 10-cm dishes (3.5 × 10^6 cells per dish) and transfected with the plasmids indicated in the Figs using PEI. The following day, cells were washed twice with PSB, lysed in immunoprecipitation (IP) lysis buffer (150 mM NaCl, 50 mM Tris-HCl pH 7.4, 0.5% (v/v) Nonidet P-40 (NP-40) and protease (cOmplete Mini, Roche) and phosphatase inhibitors (PhosSTOP, Roche)) and cleared by centrifugation at 21,000 *g* for 15 min at 4 ºC). Cleared lysates were then incubated with 20 µL of ANTI-FLAG M2 Affinity Gel (Sigma Aldrich) or Anti-HA Agarose (Sigma Aldrich) for 2 h, or with 50 uL of Anti-c-Myc Agarose overnight, at 4 ºC. Alternatively, proteins were expressed by *in*

vitro transcription/translation using the TNT SP6 High-Yield Wheat Germ Protein Expression System (Promega) prior to incubation with the affinity resins. Immunoprecipitations were washed 3 or 4 times in IP buffer and bound proteins were eluted in Laemmli SDS-PAGE loading buffer and heated at 100 ºC for 5 min. Samples were then analysed by SDS-PAGE and immunoblotting.

RT-qPCR

HEK293T (4×10^5) or MEFs (1×10^5) cells were seeded in 12-well plates. The next day, cells were stimulated by infection with SeV or transfection with 5 µg/mL of poly I:C using lipofectamine 2000 (Life Technologies). RNA was extracted using the RNeasy kit (QIAGEN) and 500 ng of each RNA sample was used to synthesise cDNA using Superscript III reverse transcriptase according to the manufacturer's protocol (Invitrogen). mRNA was quantified by real-time PCR using a ViiA 7 Real-Time PCR System (Life Technologies), fast SYBR Green Master Mix (Applied Biosystems) and the following primers: human CXCL-10 (Fwd: GTGGCATTCAAGGAGTACCTC, Rev: GCCTTCGATTCTGGATTCAGA), human IFNβ (Fwd:ACATCCCTGAGGAGATTAAGCA, Rev: GCCAGGAGGTTCTCAACAATAG), human IFIT1 (Fwd: CCTGAAAGGCCAGAATGAGG, Rev: TCCACCTTGTCCAGGTAAGT), human GAPDH (Fwd: ACCCAGAAGACTGTGGATGG, Rev: TTCTAGACGGCAGGTCAGGT), mouse IFIT1 (Fwd: ACCATGGGAGAGAATGCTGAT, Rev: GCCAGGAGGTTGTGC), mouse IL6 (Fwd: GTAGCTATGGTACTCCAGAAGAC. Rev: ACGATGATGCACTTGCAGAA), mouse CXCL-10 (Fwd: ACTGCATCCATATCGATGAC, Rev: TTCATCGTGGCAATGATCTC) and mouse GAPDH (Fwd: ATGGTGAAGGTCGGTGTGAACGG, Rev: TTACTCCTTGGAGGCCATGTAGGC). Gene amplification was normalised to glyceraldehyde-3-phosphate dehydrogenase (GAPDH) amplification from the same sample, and the fold induction of genes in stimulated samples was calculated relative to the unstimulated control. Experiments were performed in at least biological duplicate and conducted at least twice.

ELISA

HEK293T (4×10^5) or MEFs (1×10^5) cells were seeded in 12-well plates. The following day, cells were stimulated by: (i) infection with SeV; (ii) transfection with 5 µg/mL of poly I:C using lipofectamine 2000 (Life Technologies), (iii) 50 ng/mL of human TNF-α or (iv) 50 ng/mL of mouse IL-1β. After stimulation, supernatants were assayed for human or murine CXCL-10 and IL-6 protein using Duoset enzyme-linked immunosorbent assay (ELISA) reagents (R&D Biosystems) according to the manufacturer’s instructions.

CRISPR/Cas9-mediated genome editing

Two guide RNAs (gRNAs) were designed using online software (http://tools.genome-engineering.org) to target *Spire1* gene exon 3, which is shared by all Spir-1 isoforms. CRISPR/Cas9-mediated genome

editing of HEK293T cells was performed as described (Ran *et al*, 2013). Briefly, px459 CRISPR/Cas9 plasmids with or without gRNA sequence were transfected into HEK293T using TransIT-LT1 transfection reagent (Mirus, MIR 2306). Puromycin (1 µg/mL) was added to transfected cells, and after 48 h, puromycin-resistant cells were serially diluted to obtain individual clones. Several clones were amplified, and a few potential knockout clones were selected by immunoblotting and confirmed by genomic DNA sequencing at the gRNA target sites. Only one gRNA was successful and one clonal cell line was confirmed to be knockout after PCR-amplified genomic DNA was cloned into bacterial plasmids and multiple colonies (n = 20) were sequenced. These all contained frameshift mutations. No wild type allele was identified.

Lentivirus transductions

Lentivirus particles for transduction were generated after transient co-transfection of HEK293T cells seeded in 6-cm dishes. Cells were transfected with pCMV.dR8.91 and pMD-G vectors together with either pLDT-EV or pLDT-Myc-Spir-1 and 48 h and 72 h later, the supernatant was collected and passed through a 0.45 µm filter. Lentivirus-containing supernatant was then used to infect HEK293T Spir-1 WT and KO cells. Transduced cells were selected with 1 µg/mL puromycin followed by clonal selection by serial dilution. Spir-1 expression was assessed by immunoblotting.

Virus Infection

Plaque size analysis were performed in HEK293T Spir-1 WT and KO cells seeded in 6-well plates coated with poly-D-lysine (Sigma). Once confluent, cells were infected with VACV-A5-GFP at 20 PFU per well for 2 d and then stained with toluidine blue. Virus plaques diameters (*n*=54) were measured using AxioVision 4.8 software and a ZEISS Axio Vert.A1 fluorescent microscope.

Viral replication was measured by multi-step growth analyses of HEK293T Spir-1 WT and KO cells infected with VACV-WR at 0.001 PFU / cell. At 48 h post infection, cells were scraped in their medium and collected by centrifugation at 500 *g* for 5 min. Cells were subjected to three rounds of freeze-thawing before the infectious viral titre was determined by plaque assay on BSC-1 cells.

Statistical Analysis

Statistical analysis were carried out using one or two-way ANOVA test where appropriate with the Bonferroni post-test, using the GraphPad Prism statistical software (Graph-Pad Software). Statistical significance is expressed as follows: ns = not significant, *P < 0.05, **P < 0.01, ***P < 0.001, ****P < 0.0001.

Acknowledgements.

This work was supported by grant 090315 from the Wellcome Trust.

Conflicts of Interest.

The authors declare that they have no conflict of interest.

References

Alzahofi N, Welz T, Robinson CL, Page EL, Briggs DA, Stainthorp AK, Reekes J, Elbe DA, Straub F, Kallemeijn WW *et al* (2020) Rab27a co-ordinates actin-dependent transport by controlling organelle-associated motors and track assembly proteins. *Nat Commun* 11: 3495

Belin BJ, Lee T, Mullins RD (2015) DNA damage induces nuclear actin filament assembly by Formin -2 and Spire-(1/2) that promotes efficient DNA repair. [corrected]. *Elife* 4: e07735

Benfield CTO, Ren H, Lucas SJ, Bahsoun B, Smith GL (2013) Vaccinia virus protein K7 is a virulence factor that alters the acute immune response to infection. *J Gen Virol* 94: 1647-1657

Benzinger A, Muster N, Koch HB, Yates JR, 3rd, Hermeking H (2005) Targetted proteomic analysis of 14-3-3 sigma, a p53 effector commonly silenced in cancer. *Mol Cell Proteomics* 4: 785-795

Bosch M, Le KH, Bugyi B, Correia JJ, Renault L, Carlier MF (2007) Analysis of the function of Spire in actin assembly and its synergy with formin and profilin. *Mol Cell* 28: 555-568

Brisse M, Ly H (2019) Comparative Structure and Function Analysis of the RIG-I-Like Receptors: RIG-I and MDA5. *Front Immunol* 10: 1586

Carpentier DC, Gao WN, Ewles H, Morgan GW, Smith GL (2015) Vaccinia virus protein complex F12/E2 interacts with kinesin light chain isoform 2 to engage the kinesin-1 motor complex. *PLoS Pathog* 11: e1004723

Carter GC, Rodger G, Murphy BJ, Law M, Krauss O, Hollinshead M, Smith GL (2003) Vaccinia virus cores are transported on microtubules. *J Gen Virol* 84: 2443-2458

Chen RA, Jacobs N, Smith GL (2006) Vaccinia virus strain Western Reserve protein B14 is an intracellular virulence factor. *J Gen Virol* 87: 1451-1458

Chen RA, Ryzhakov G, Cooray S, Randow F, Smith GL (2008) Inhibition of IkappaB kinase by vaccinia virus virulence factor B14. *PLoS Pathog* 4: e22

Colby C, Duesberg PH (1969) Double-stranded RNA in vaccinia virus infected cells. *Nature* 222: 940-944

Ducka AM, Joel P, Popowicz GM, Trybus KM, Schleicher M, Noegel AA, Huber R, Holak TA, Sitar T (2010) Structures of actin-bound Wiskott-Aldrich syndrome protein homology 2 (WH2) domains of Spire and the implication for filament nucleation. *Proc Natl Acad Sci U S A* 107: 11757-11762

Everett RD, Bell AJ, Lu Y, Orr A (2013) The replication defect of ICP0-null mutant herpes simplex virus 1 can be largely complemented by the combined activities of human cytomegalovirus proteins IE1 and pp71. *J Virol* 87: 978-990

Everett RD, Parsy ML, Orr A (2009) Analysis of the functions of herpes simplex virus type 1 regulatory protein ICP0 that are critical for lytic infection and derepression of quiescent viral genomes. *J Virol* 83: 4963-4977

Ewing RM, Chu P, Elisma F, Li H, Taylor P, Climie S, McBroom-Cerajewski L, Robinson MD, O'Connor L, Li M *et al* (2007) Large-scale mapping of human protein-protein interactions by mass spectrometry. *Mol Syst Biol* 3: 89

Fenner F, Henderson DA, Arita I, Jezek Z, Ladnyi ID (1988) Smallpox and its eradication. *World Health Organisation, Geneva*

Ferguson BJ, Benfield CTO, Ren H, Lee VH, Frazer GL, Strnadova P, Sumner RP, Smith GL (2013) Vaccinia virus protein N2 is a nuclear IRF3 inhibitor that promotes virulence. *J Gen Virol* 94: 2070-2081

Fullam A, Schroder M (2013) DExD/H-box RNA helicases as mediators of anti-viral innate immunity and essential host factors for viral replication. *Biochim Biophys Acta* 1829: 854-865

Garcia-Sastre A (2017) Ten Strategies of Interferon Evasion by Viruses. *Cell Host Microbe* 22: 176-184

Goebel SJ, Johnson GP, Perkus ME, Davis SW, Winslow JP, Paoletti E (1990) The complete DNA sequence of vaccinia virus. *Virology* 179: 247-266, 517-263

Gu L, Fullam A, McCormack N, Hohn Y, Schroder M (2017) DDX3 directly regulates TRAF3 ubiquitination and acts as a scaffold to co-ordinate assembly of signalling complexes downstream from MAVS. *Biochem J* 474: 571-587

Janeway CA, Jr., Medzhitov R (2002) Innate immune recognition. *Annu Rev Immunol* 20: 197-216

Kalverda AP, Thompson GS, Vogel A, Schroder M, Bowie AG, Khan AR, Homans SW (2009) Poxvirus K7 protein adopts a Bcl-2 fold: biochemical mapping of its interactions with human DEAD box RNA helicase DDX3. *J Mol Biol* 385: 843-853

Kato H, Sato S, Yoneyama M, Yamamoto M, Uematsu S, Matsui K, Tsujimura T, Takeda K, Fujita T, Takeuchi O *et al* (2005) Cell type-specific involvement of RIG-I in antiviral response. *Immunity* 23: 19-28

Kato H, Takeuchi O, Mikamo-Satoh E, Hirai R, Kawai T, Matsushita K, Hiiragi A, Dermody TS, Fujita T, Akira S (2008) Length-dependent recognition of double-stranded ribonucleic acids by retinoic acid-inducible gene-I and melanoma differentiation-associated gene 5. *J Exp Med* 205: 1601-1610

Kato H, Takeuchi O, Sato S, Yoneyama M, Yamamoto M, Matsui K, Uematsu S, Jung A, Kawai T, Ishii KJ *et al* (2006) Differential roles of MDA5 and RIG-I helicases in the recognition of RNA viruses. *Nature* 441: 101-105

Kerkhoff E (2006) Cellular functions of the Spir actin-nucleation factors. *Trends Cell Biol* 16: 477-483

Kerkhoff E, Simpson JC, Leberfinger CB, Otto IM, Doerks T, Bork P, Rapp UR, Raabe T, Pepperkok R (2001) The Spir actin organizers are involved in vesicle transport processes. *Curr Biol* 11: 1963-1968

Kollmar M, Welz T, Straub F, Alzahofi N, Hatje K, Briggs DA, Samol-Wolf A, Burkhardt P, Hume H, Kerkhoff E (2020) Animal evolution coincides with a novel degree of freedom in exocytic transport processes. *bioRxiv* https://doi.org/10.1101/591974

Lagal V, Abrivard M, Gonzalez V, Perazzi A, Popli S, Verzeroli E, Tardieux I (2014) Spire-1 contributes to the invadosome and its associated invasive properties. *J Cell Sci* 127: 328-340

Li Y, Zhang L, Ke Y (2017) Cellular interactome analysis of vaccinia virus K7 protein identifies three transport machineries as binding partners for K7. *Virus Genes* 53: 814-822

Liu SW, Katsafanas GC, Liu R, Wyatt LS, Moss B (2015) Poxvirus decapping enzymes enhance virulence by preventing the accumulation of dsRNA and the induction of innate antiviral responses. *Cell Host Microbe* 17: 320-331

Liu Y, Olagnier D, Lin R (2016) Host and Viral Modulation of RIG-I-Mediated Antiviral Immunity. *Front Immunol* 7: 662

Lu Y, Stuart JH, Talbot-Cooper C, Agrawal-Singh S, Huntly B, Smid AI, Snowden JS, Dupont L, Smith GL (2019) Histone deacetylase 4 promotes type I interferon signaling, restricts DNA viruses, and is degraded via vaccinia virus protein C6. *Proc Natl Acad Sci U S A* 116: 11997-12006

Manor U, Bartholomew S, Golani G, Christenson E, Kozlov M, Higgs H, Spudich J, Lippincott-Schwartz J (2015) A mitochondria-anchored isoform of the actin-nucleating spire protein regulates mitochondrial division. *Elife* 4

Manseau LJ, Schupbach T (1989) cappuccino and spire: two unique maternal-effect loci required for both the anteroposterior and dorsoventral patterns of the Drosophila embryo. *Genes Dev* 3: 1437-1452

Mansur DS, Maluquer de Motes C, Unterholzner L, Sumner RP, Ferguson BJ, Ren H, Strnadova P, Bowie AG, Smith GL (2013) Poxvirus targetting of E3 ligase beta-TrCP by molecular mimicry: a mechanism to inhibit NF-kappaB activation and promote immune evasion and virulence. *PLoS Pathog* 9: e1003183

Marq JB, Hausmann S, Luban J, Kolakofsky D, Garcin D (2009) The double-stranded RNA binding domain of the vaccinia virus E3L protein inhibits both RNA- and DNA-induced activation of interferon beta. *J Biol Chem* 284: 25471-25478

Montaville P, Jegou A, Pernier J, Compper C, Guichard B, Mogessie B, Schuh M, Romet-Lemonne G, Carlier MF (2014) Spire and Formin 2 synergize and antagonize in regulating actin assembly in meiosis by a ping-pong mechanism. *PLoS Biol* 12: e1001795

Morel E, Parton RG, Gruenberg J (2009) Annexin A2-dependent polymerization of actin mediates endosome biogenesis. *Dev Cell* 16: 445-457

Moss B (2013) Poxviridae. In: *Fields Virology*, Knipe D.M.H., P. M. (ed.) pp. 2129-2159. Lippincott Williams & Wilkins: Philadelphia

Neidel S, Maluquer de Motes C, Mansur DS, Strnadova P, Smith GL, Graham SC (2015) Vaccinia virus protein A49 is an unexpected member of the B-cell Lymphoma (Bcl)-2 protein family. *J Biol Chem* 290: 5991-6002

Neidel S, Torres AA, Ren H, Smith GL (2020) Leaky scanning translation generates a second A49 protein that contributes to vaccinia virus virulence. *J Gen Virol* 101: 533-541

Oda S, Schroder M, Khan AR (2009) Structural basis for targetting of human RNA helicase DDX3 by poxvirus protein K7. *Structure* 17: 1528-1537

Odon V, Georgana I, Holley J, Morata J, Maluquer de Motes C (2018) Novel Class of Viral Ankyrin Proteins Targetting the Host E3 Ubiquitin Ligase Cullin-2. *J Virol* 92

Ovsyannikova IG, Kennedy RB, O'Byrne M, Jacobson RM, Pankratz VS, Poland GA (2012) Genome-wide association study of antibody response to smallpox vaccine. *Vaccine* 30: 4182-4189

Pang IK, Iwasaki A (2012) Control of antiviral immunity by pattern recognition and the microbiome. *Immunol Rev* 245: 209-226

Pechlivanis M, Samol A, Kerkhoff E (2009) Identification of a short Spir interaction sequence at the C-terminal end of formin subgroup proteins. *J Biol Chem* 284: 25324-25333

Pfender S, Kuznetsov V, Pleiser S, Kerkhoff E, Schuh M (2011) Spire-type actin nucleators cooperate with Formin-2 to drive asymmetric oocyte division. *Curr Biol* 21: 955-960

Pichlmair A, Kandasamy K, Alvisi G, Mulhern O, Sacco R, Habjan M, Binder M, Stefanovic A, Eberle CA, Goncalves A *et al* (2012) Viral immune modulators perturb the human molecular network by common and unique strategies. *Nature* 487: 486-490

Pichlmair A, Schulz O, Tan CP, Rehwinkel J, Kato H, Takeuchi O, Akira S, Way M, Schiavo G, Reis e Sousa C (2009) Activation of MDA5 requires higher-order RNA structures generated during virus infection. *J Virol* 83: 10761-10769

Pleiser S, Banchaabouchi MA, Samol-Wolf A, Farley D, Welz T, Wellbourne-Wood J, Gehring I, Linkner J, Faix J, Riemenschneider MJ *et al* (2014) Enhanced fear expression in Spir-1 actin organizer mutant mice. *Eur J Cell Biol* 93: 225-237

Pleiser S, Rock R, Wellmann J, Gessler M, Kerkhoff E (2010) Expression patterns of the mouse Spir-2 actin nucleator. *Gene Expr Patterns* 10: 345-350

Pylypenko O, Welz T, Tittel J, Kollmar M, Chardon F, Malherbe G, Weiss S, Michel CI, Samol-Wolf A, Grasskamp AT *et al* (2016) Coordinated recruitment of Spir actin nucleators and myosin V motors to Rab11 vesicle membranes. *Elife* 5

Quinlan ME (2013) Direct interaction between two actin nucleators is required in Drosophila oogenesis. *Development* 140: 4417-4425

Quinlan ME, Heuser JE, Kerkhoff E, Mullins RD (2005) Drosophila Spire is an actin nucleation factor. *Nature* 433: 382-388

Quinlan ME, Hilgert S, Bedrossian A, Mullins RD, Kerkhoff E (2007) Regulatory interactions between two actin nucleators, Spire and Cappuccino. *J Cell Biol* 179: 117-128

Ran FA, Hsu PD, Wright J, Agarwala V, Scott DA, Zhang F (2013) Genome engineering using the CRISPR-Cas9 system. *Nat Protoc* 8: 2281-2308

Randall RE, Goodbourn S (2008) Interferons and viruses: an interplay between induction, signalling, antiviral responses and virus countermeasures. *J Gen Virol* 89: 1-47

Rice AP, Roberts WK, Kerr IM (1984) 2-5A accumulates to high levels in interferon-treated, vaccinia virus-infected cells in the absence of any inhibition of virus replication. *J Virol* 50: 220-228

Schroder M, Baran M, Bowie AG (2008) Viral targetting of DEAD box protein 3 reveals its role in TBK1/IKKepsilon-mediated IRF activation. *EMBO J* 27: 2147-2157

Schuh M (2011) An actin-dependent mechanism for long-range vesicle transport. *Nat Cell Biol* 13: 1431-1436

Schumacher N, Borawski JM, Leberfinger CB, Gessler M, Kerkhoff E (2004) Overlapping expression pattern of the actin organizers Spir-1 and formin-2 in the developing mouse nervous system and the adult brain. *Gene Expr Patterns* 4: 249-255

Seth RB, Sun L, Ea CK, Chen ZJ (2005) Identification and characterization of MAVS, a mitochondrial antiviral signaling protein that activates NF-kappaB and IRF 3. *Cell* 122: 669-682

Sitar T, Gallinger J, Ducka AM, Ikonen TP, Wohlhoefler M, Schmoller KM, Bausch AR, Joel P, Trybus KM, Noegel AA *et al* (2011) Molecular architecture of the Spire-actin nucleus and its implication for actin filament assembly. *Proc Natl Acad Sci U S A* 108: 19575-19580

Smith GL, Benfield CTO, Maluquer de Motes C, Mazzon M, Ember SWJ, Ferguson BJ, Sumner RP (2013) Vaccinia virus immune evasion: mechanisms, virulence and immunogenicity. *J Gen Virol* 94: 2367-2392

Smith GL, Vanderplasschen A, Law M (2002) The formation and function of extracellular enveloped vaccinia virus. *J Gen Virol* 83: 2915-2931

Soday L, Lu Y, Albarnaz JD, Davies CTR, Antrobus R, Smith GL, Weekes MP (2019) Quantitative Temporal Proteomic Analysis of Vaccinia Virus Infection Reveals Regulation of Histone Deacetylases by an Interferon Antagonist. *Cell Rep* 27: 1920-1933 e1927

Soulat D, Burckstummer T, Westermayer S, Goncalves A, Bauch A, Stefanovic A, Hantschel O, Bennett KL, Decker T, Superti-Furga G (2008) The DEAD-box helicase DDX3X is a critical component of the TANK-binding kinase 1-dependent innate immune response. *EMBO J* 27: 2135-2146

Stinski MF, Meier JL (2007) Immediate-early viral gene regulation and function. In: *Human Herpesviruses: Biology, Therapy, and Immunoprophylaxis*, Arvin A., Campadelli-Fiume G., Mocarski E., Moore P.S., Roizman B., Whitley R., Yamanishi K. (eds.)Cambridge

Stuart JH, Sumner RP, Lu Y, Snowden JS, Smith GL (2016) Vaccinia Virus Protein C6 Inhibits Type I IFN Signalling in the Nucleus and Binds to the Transactivation Domain of STAT2. *PLoS Pathog* 12: e1005955

Teferi WM, Desaulniers MA, Noyce RS, Shenouda M, Umer B, Evans DH (2017) The vaccinia virus K7 protein promotes histone methylation associated with heterochromatin formation. *PLoS One* 12: e0173056

Thompson MR, Kaminski JJ, Kurt-Jones EA, Fitzgerald KA (2011) Pattern recognition receptors and the innate immune response to viral infection. *Viruses* 3: 920-940

Tittel J, Welz T, Czogalla A, Dietrich S, Samol-Wolf A, Schulte M, Schwille P, Weidemann T, Kerkhoff E (2015) Membrane targetting of the Spir.formin actin nucleator complex requires a sequential handshake of polar interactions. *J Biol Chem* 290: 6428-6444

Torres AA, Albarnaz JD, Bonjardim CA, Smith GL (2016) Multiple Bcl-2 family immunomodulators from vaccinia virus regulate MAPK/AP-1 activation. *J Gen Virol* 97: 2346-2351

Unterholzner L, Sumner RP, Baran M, Ren H, Mansur DS, Bourke NM, Randow F, Smith GL, Bowie AG (2011) Vaccinia virus protein C6 is a virulence factor that binds TBK-1 adaptor proteins and inhibits activation of IRF3 and IRF7. *PLoS Pathog* 7: e1002247

Valentine R, Smith GL (2010) Inhibition of the RNA polymerase III-mediated dsDNA-sensing pathway of innate immunity by vaccinia virus protein E3. *J Gen Virol* 91: 2221-2229

Vizcarra CL, Kreutz B, Rodal AA, Toms AV, Lu J, Zheng W, Quinlan ME, Eck MJ (2011) Structure and function of the interacting domains of Spire and Fmn-family formins. *Proc Natl Acad Sci U S A* 108: 11884-11889

Wang T, Birsoy K, Hughes NW, Krupczak KM, Post Y, Wei JJ, Lander ES, Sabatini DM (2015) Identification and characterization of essential genes in the human genome. *Science* 350: 1096-1101

Weber F, Wagner V, Rasmussen SB, Hartmann R, Paludan SR (2006) Double-stranded RNA is produced by positive-strand RNA viruses and DNA viruses but not in detectable amounts by negative-strand RNA viruses. *J Virol* 80: 5059-5064

Wellington A, Emmons S, James B, Calley J, Grover M, Tolias P, Manseau L (1999) Spire contains actin binding domains and is related to ascidian posterior end mark-5. *Development* 126: 5267-5274

Wen Q, Li N, Xiao X, Lui WY, Chu DS, Wong CKC, Lian Q, Ge R, Lee WM, Silvestrini B *et al* (2018) Actin nucleator Spire 1 is a regulator of ectoplasmic specialization in the testis. *Cell Death Dis* 9: 208

Zeth K, Pechlivanis M, Samol A, Pleiser S, Vonrhein C, Kerkhoff E (2011) Molecular basis of actin nucleation factor cooperativity: crystal structure of the Spir-1 kinase non-catalytic C-lobe domain (KIND)*formin-2 formin SPIR interaction motif (FSI) complex. *J Biol Chem* 286: 30732-30739

Figure Legends

Fig. 1: Spir-1 co-immunoprecipitates VACV protein K7 via its C-terminal region. HEK293T cells were transfected (**A**, **B** and **D**) with Myc-tagged and FLAG-tagged plasmids overnight. Cell lysates were immunoprecipitated using either Myc (**A** and **D** – right panel) or FLAG affinity resins (**B** and **D** – middle panel) and analysed by SDS-PAGE and immunoblotting. (**C**) Schematic representations of hSpir-1 isoform 2 full-length (top) and its C- and N-terminal truncations. (**E**) HEK293T cells were either mock-infected or infected at 5 or 10 PFU/cell with vHA-K7 or vHA-B14 for 4 h. Lysates were immunoprecipitated using HA-affinity resin and analysed by SDS-PAGE and immunoblotting. In (**A**), (**B**), (**D**) and (**E**) the positions of molecular mass markers in kDa are shown on the left. Each experiment was done 3 times and representative results are shown.

Fig. 2: **Ectopic expression of Spir-1 increases IRF3-dependent gene expression induced by other stimuli, at or downstream of MAVS.** HEK293T cells were transfected with IFNβ (**A**), ISRE (**B**) and NF-κB (**C**) firefly luciferase reporter plasmids, together with TK-renilla luciferase and 40 ng of the plasmids for expression of the indicated proteins. After overnight transfection, cells were stimulated with SeV for 24 h (**A**), IFNα (**B**) or TNF-α (**C**) for 8 h. **D-I**) HEK293T cells were transfected with the ISG56.1 firefly luciferase reporter plasmid, TK-renilla luciferase and plasmids for expression of the indicated proteins. Cells were also co-transfected with EV as the non-stimulated (NS) controls or with the 5 ng of CARD-domain of RIG-I (**D**, **E** and **I**), 40 ng of MAVS (**F**), 40 ng of TBK-1 (**G**) and 5 ng of

IRF3-5D (**H**) plasmids to activate the IRF3 pathway. EV was added to samples when necessary to keep the final amount of DNA transfected as 40 ng in all samples. Cell lysates were prepared and luciferase expression was measured and normalised to renilla luciferase. At least triplicate samples were analysed for each condition. Data are expressed as the mean (± SEM) fold induction of the firefly luciferase activity normalised to renilla values for the stimulated versus non-stimulated samples. Data shown are representative of three independent experiments. Immunoblots underneath each graph show the expression levels of the different proteins. The positions of molecular mass markers in kDa are shown on the right and the antibodies used are shown on the left. ns = not significant; *P < 0.05; ****P < 0.0001.

Fig. 3: Spir-1 and DDX3 share a conserved diphenylalanine motif that is required for IRF3 activation and direct binding to K7. (**A**) DDX3 knockdown was induced in HEK293T cells stably transfected with pTRIPZ-shDDX3 (or a NSC pTRIPZ vector) through incubation with doxycycline for 48 h. Twenty-four h after doxycycline addition, cells were transfected with FLAG-tagged plasmids overnight. Cell lysates were immunoprecipitated using FLAG-affinity resin and analysed by SDS-PAGE and immunoblotting. (**B**) DDX3 knockdown was induced in HEK293T shDDX3 cells as in (**A**) and cells were then transfected with ISG56.1-firefly luciferase reporter, TK-renilla luciferase, plasmids for expression of the indicated proteins together with the CARD-domain. Cell lysates were prepared and analysed as in Fig. 2. Immunoblots underneath the graph show the expression levels of the different proteins. (**C**) Alignment of amino acid residues of Spir-1 and DDX3 showing the conserved diphenylalanine motif. (**D**) HEK293T cells were transfected overnight with Myc-tagged Spir-1 wild type, GFP or Spir-1 mutant FFAA together with FLAG-K7. Cell lysates were immunoprecipitated using either Myc (middle panel) or FLAG-affinity resins (right panel) and analysed by SDS-PAGE and immunoblotting. (**E**) HEK293T cells were transfected with ISG56.1 firefly luciferase reporter, TK-renilla luciferase, plasmids for expression of the indicated proteins together with the CARD-domain of RIG-I or EV as the NS control. Cell lysates were prepared and analysed as in (**B**). The panel underneath the graph shows immunoblots for the expression level of K7 and GAPDH. (**F**, **G**) Myc or FLAG-tagged proteins were synthesized by *in vitro* transcription/translation. Samples were immunoprecipitated using FLAG- (**F**) or Myc-affinity resins (**G**) and analysed by SDS-PAGE and immunoblotting. For all immunoblots, the positions of molecular mass markers in kDa are shown on the left and the antibodies used on the right. ns = not significant; ****P < 0.0001. HC/LC: IgG heavy chain or light chain, respectively.

Fig. 4: K7 residue Asp31 is important for binding to Spir-1 and DDX3 and inhibition of IRF3 activation. HEK293T cells were transfected with FLAG-tagged GFP, K7 wild type or mutants, Myc-Spir-1 and HA-DDX3 (**A**) or with only FLAG-tagged plasmids overnight (**B**). Cell lysates were immunoprecipitated using FLAG-affinity resin and analysed by SDS-PAGE and immunoblotting. The

positions of molecular mass markers in kDa are shown on the left and the antibodies used on the right. (**C**) HEK293T cells were transfected with ISG56.1-firefly luciferase reporter, TK-renilla luciferase, plasmids for expression of the indicated proteins together with the CARD-domain or EV as the NS control. Cell lysates were prepared and analysed as in Fig. 2. Statistical analyses compared the fold induction of the mutant sample to its respective K7 wild type. The panel underneath the graph shows immunoblots for the expression levels of the different K7 proteins and α-tubulin. The positions of molecular mass markers in kDa are shown on the right and the antibodies used on the left. ns = not significant; ****P < 0.0001. LC: IgG light chain.

Fig. 5: Spir-1 contributes to IRF3 phosphorylation and IRF3 stimulated gene expression after SeV infection in HEK293T cells. (**A**) Schematic of CRISPR-Cas9-mediated knockout strategy targetting *Spire1* exon 3 and single allele sequences of HEK293T Spir-1 knockout (KO) cells. (**B-F**) Spir-1 knockout (KO) HEK293T cells were transduced with empty vector (EV) or Myc-Spir-1 lentiviruses to rescue Spir-1 expression. Cells lines were either non-infected (NS) or infected with SeV for the indicated times. Cells were then either lysed and analysed by immunoblotting (**B**) or subjected to total RNA extraction followed by RT-qPCR (**C-E**). Supernatants were analysed by ELISA (**F**). (**G**) Spir-1 KO or wild type (WT) HEK293T cells were stimulated overnight with TNF**α** and supernatants were analysed by ELISA. ns = not significant, **P < 0.01, ***P < 0.001, ****P < 0.0001.

Fig. 6: IRF3 activation is reduced in Spir-1 KO MEFs. Spir-1 WT or KO MEF cells were transfected with poly I:C (**A, C-E, I-J**) or infected with SeV (**B, F-H, K-L**) for the indicated times. Cells were lysed and analysed by immunoblotting (**A, B**) and phospho-IRF3 bands intensity was quantified and normalised by the intensity of tubulin from three different experiments (**A**, **G**, bottom graphs). The positions of molecular mass markers in kDa are shown on the left and the antibodies used on the right. Cells were also subjected to total RNA extraction followed by RT-qPCR (C-H) and supernatants were analysed by ELISA (**I-L**). (**M, N**) Spir-1 WT or KO MEF cells were stimulated with IL-1β for 8 h and supernatants were analysed by ELISA. ns = not significant, *P < 0.05, **P < 0.01, ****P < 0.0001.

Fig. 7: Spir-1 is a cellular restriction factor for VACV. (**A, B**) Spir-1 WT or KO and Spir-1 KO complemented HEK293T cells were infected with VACV-A5-GFP and plaque diameters were measured at 48 h p.i. (**A**) Representative plaques formed in each cell line. (**B**) Plaques diameter measurements (n=54). (**C**) Spir-1 WT or KO and Spir-1 KO complemented HEK293T cells were infected with VACV WR at 0.001 PFU/cell for 48 h and the virus yield was measured in BSC-1 cells. ns = not significant, *P<0.05, **P < 0.01, ***P < 0.001, ****P < 0.0001.

Expanded View Fig. Legend

Fig. EV1: **Ectopic expression of Spir-1 doesn't affect IRF3-dependent gene expression induced by IKKε (related to Figure 2).** HEK293T cells was transfected with the ISG56.1 firefly luciferase reporter plasmid, TK-renilla luciferase and plasmids for expression of the indicated proteins. Cells were also co-transfected with EV as the non-stimulated (NS) controls or with the 100 ng of IKKε plasmid to activate the IRF3 pathway. EV was added to samples when necessary to keep the final amount of DNA transfected as 40 ng in all samples. Cell lysates were prepared and luciferase expression was measured and normalised to renilla luciferase. At least triplicate samples were analysed for each condition. Data are expressed as the mean (± SEM) fold induction of the firefly luciferase activity normalised to renilla values for the stimulated versus non-stimulated samples. Data shown are representative of three independent experiments. Immunoblots underneath each graph show the expression levels of the different proteins. The positions of molecular mass markers in kDa are shown on the right and the antibodies used are shown on the left. ns = not significant; *P < 0.05; ****P < 0.0001.

Figure 1

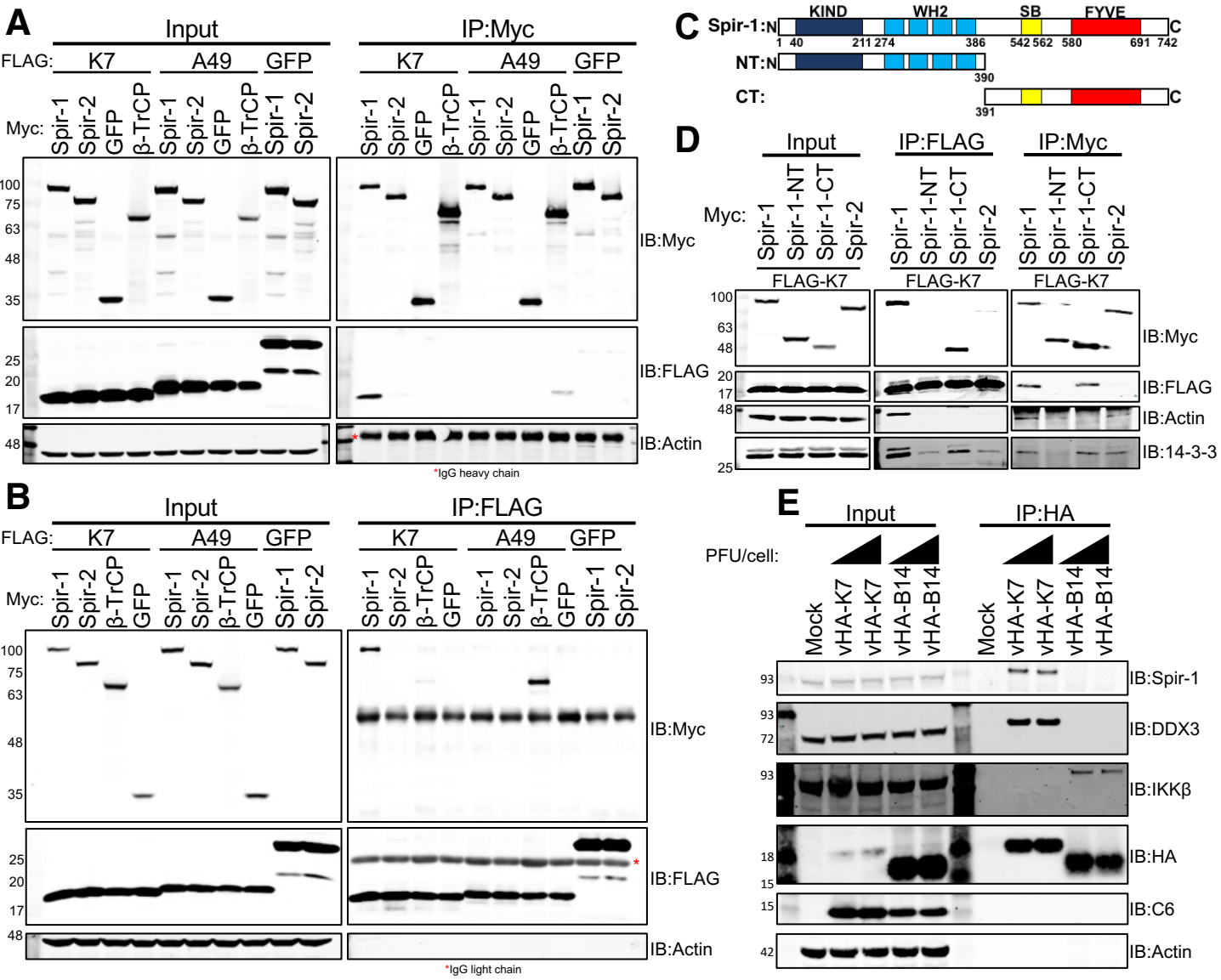
A
Input
IP:Myc
FLAG:
K7
A49
GFP
Myc:
Spir-1
Spir-2
GFP
β-TrCP
IB:Myc
IB:FLAG
IB:Actin
*IgG heavy chain
B
IP:FLAG
*IgG light chain
C
Spir-1:N
KIND
WH2
SB
FYVE
C
NT:N
CT:
D
Spir-1-NT
Spir-1-CT
FLAG-K7
IB:14-3-3
E
PFU/cell:
Mock
vHA-K7
vHA-B14
IP:HA
IB:Spir-1
IB:DDX3
IB:IKKβ
IB:HA
IB:C6

Figure 2

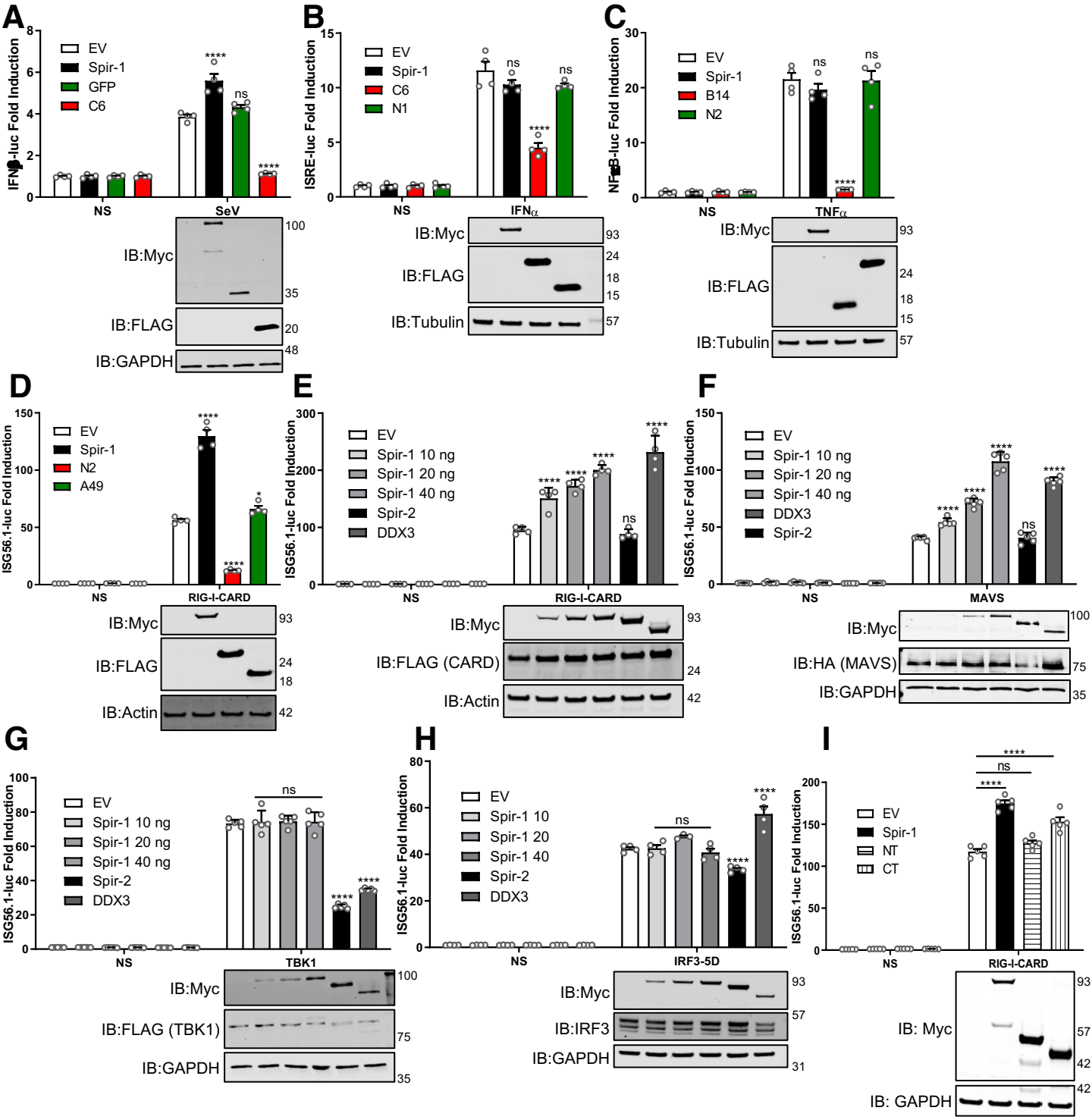
A
IFNβ-luc Fold Induction
EV
Spir-1
GFP
C6
NS
SeV
IB:Myc
IB:FLAG
IB:GAPDH
B
ISRE-luc Fold Induction
EV
Spir-1
C6
N1
NS
IFNα
IB:Myc
IB:FLAG
IB:Tubulin
C
NFκB-luc Fold Induction
EV
Spir-1
B14
N2
NS
TNFα
IB:Myc
IB:FLAG
IB:Tubulin
D
ISG56.1-luc Fold Induction
EV
Spir-1
N2
A49
NS
RIG-I-CARD
IB:Myc
IB:FLAG
IB:Actin
E
ISG56.1-luc Fold Induction
EV
Spir-1 10 ng
Spir-1 20 ng
Spir-1 40 ng
Spir-2
DDX3
NS
RIG-I-CARD
IB:Myc
IB:FLAG (CARD)
IB:Actin
F
ISG56.1-luc Fold Induction
EV
Spir-1 10 ng
Spir-1 20 ng
Spir-1 40 ng
DDX3
Spir-2
NS
MAVS
IB:Myc
IB:HA (MAVS)
IB:GAPDH
G
ISG56.1-luc Fold Induction
EV
Spir-1 10 ng
Spir-1 20 ng
Spir-1 40 ng
Spir-2
DDX3
NS
TBK1
IB:Myc
IB:FLAG (TBK1)
IB:GAPDH
H
ISG56.1-luc Fold Induction
EV
Spir-1 10
Spir-1 20
Spir-1 40
Spir-2
DDX3
NS
IRF3-5D
IB:Myc
IB:IRF3
IB:GAPDH
I
ISG56.1-luc Fold Induction
EV
Spir-1
NT
CT
NS
RIG-I-CARD
IB: Myc
IB: GAPDH

Figure 3

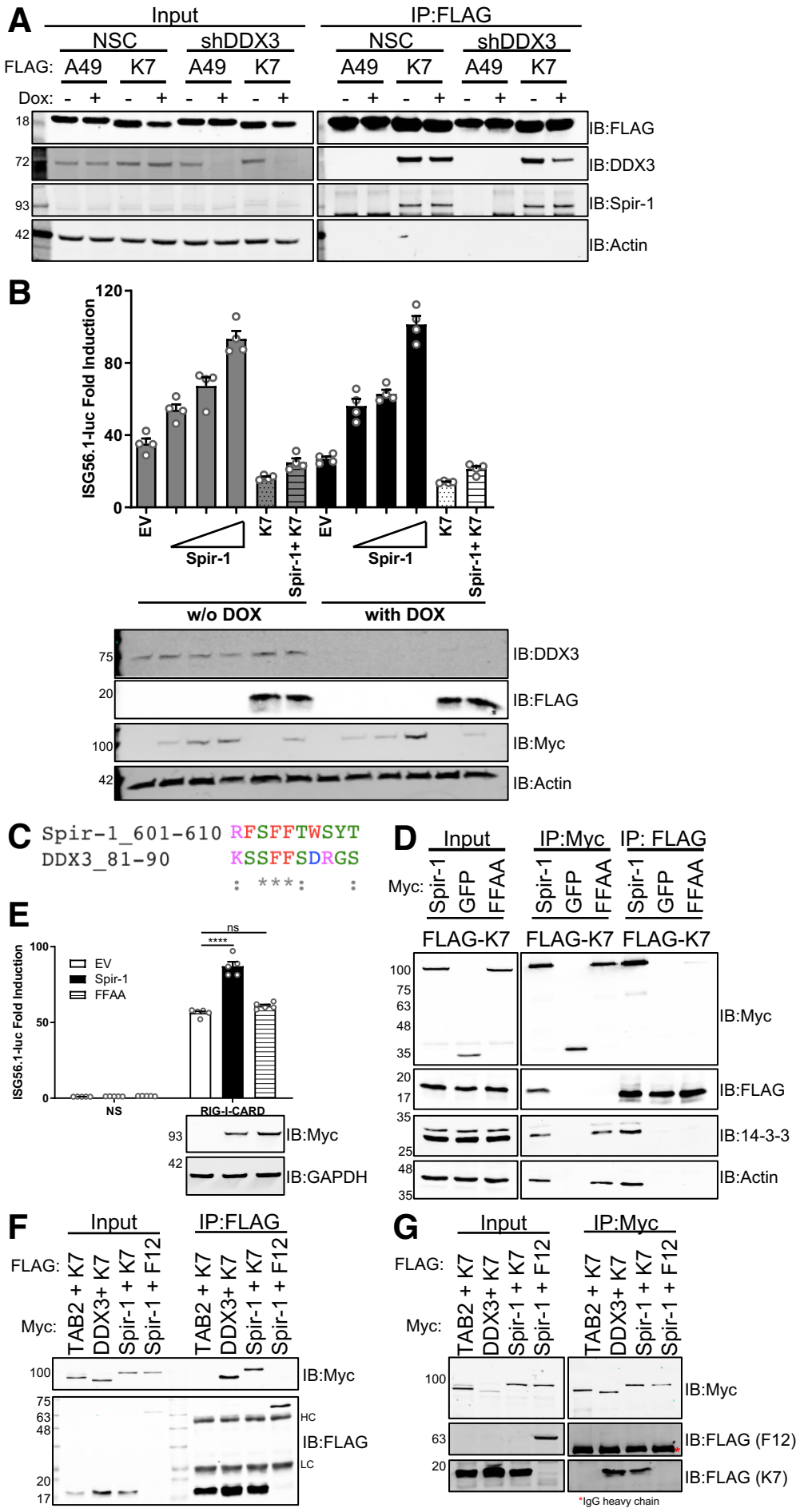
A
Input
IP:FLAG
NSC
shDDX3
FLAG: A49 K7 A49 K7
Dox: - + - + - + - +
18
72
93
42
IB:FLAG
IB:DDX3
IB:Spir-1
IB:Actin
B
ISG56.1-luc Fold Induction
120
80
40
0
EV
Spir-1
K7
Spir-1+ K7
w/o DOX
with DOX
75
20
100
42
IB:DDX3
IB:FLAG
IB:Myc
IB:Actin
C
Spir-1_601-610 RFSFFTWSYT
DDX3_81-90 KSSFFSDRGS
: ***: :
D
Input
IP:Myc
IP: FLAG
Myc: Spir-1 GFP FFAA Spir-1 GFP FFAA Spir-1 GFP FFAA
FLAG-K7 FLAG-K7 FLAG-K7
100
75
63
48
35
20
17
25
IB:Myc
IB:FLAG
IB:14-3-3
IB:Actin
E
ISG56.1-luc Fold Induction
100
50
0
EV
Spir-1
FFAA
ns
****
NS
RIG-I-CARD
93
42
IB:Myc
IB:GAPDH
F
Input
IP:FLAG
FLAG: TAB2 + K7 DDX3+ K7 Spir-1 + K7 Spir-1 + F12 TAB2 + K7 DDX3+ K7 Spir-1 + K7 Spir-1 + F12
Myc:
100
75
63
48
20
17
HC
LC
IB:Myc
IB:FLAG
G
Input
IP:Myc
FLAG: TAB2 + K7 DDX3+ K7 Spir-1 + K7 Spir-1 + F12 TAB2 + K7 DDX3+ K7 Spir-1 + K7 Spir-1 + F12
Myc:
100
63
20
IB:Myc
IB:FLAG (F12)
IB:FLAG (K7)
*IgG heavy chain

Figure 4

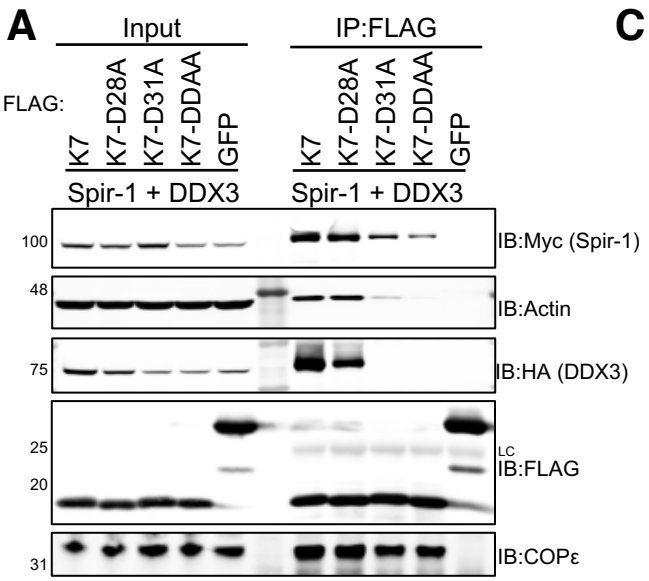
A
Input
IP:FLAG
FLAG:
K7
K7-D28A
K7-D31A
K7-DDAA
GFP
Spir-1 + DDX3
100
48
75
25
20
31
IB:Myc (Spir-1)
IB:Actin
IB:HA (DDX3)
LC
IB:FLAG
IB:COPε

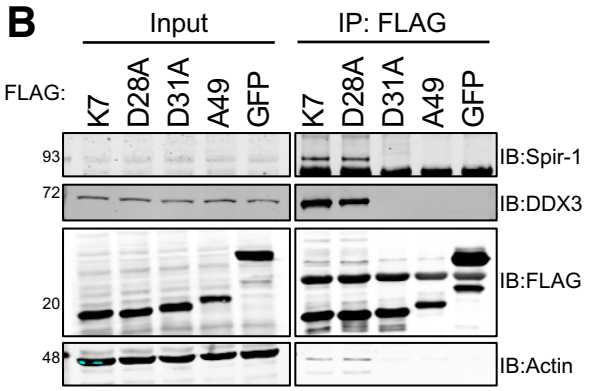
B
Input
IP: FLAG
FLAG:
K7
D28A
D31A
A49
GFP
93
72
20
48
IB:Spir-1
IB:DDX3
IB:FLAG
IB:Actin

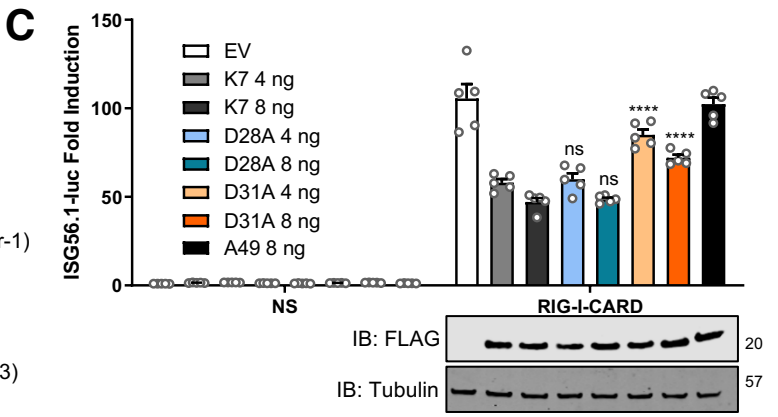
C
ISG56.1-luc Fold Induction
150
100
50
0
EV
K7 4 ng
K7 8 ng
D28A 4 ng
D28A 8 ng
D31A 4 ng
D31A 8 ng
A49 8 ng
ns
ns
****
****
NS
RIG-I-CARD
IB: FLAG
IB: Tubulin
20
57

Figure 5

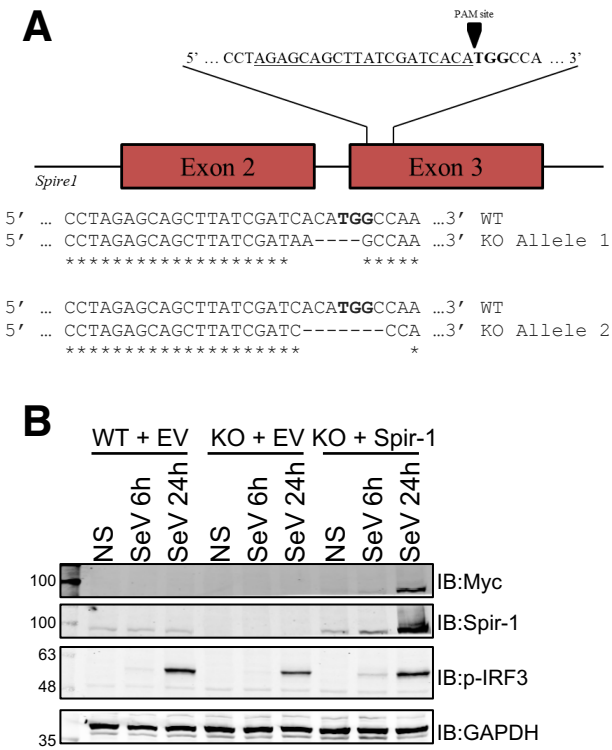
A
PAM site
5' … CCTAGAGCAGCTTATCGATCACATGGCCA … 3'
Exon 2
Exon 3
Spire1
5′ … CCTAGAGCAGCTTATCGATCACATGGCCAA …3′ WT
5′ … CCTAGAGCAGCTTATCGATAA----GCCAA …3′ KO Allele 1
5′ … CCTAGAGCAGCTTATCGATCACATGGCCAA …3′ WT
5′ … CCTAGAGCAGCTTATCGATC-------CCA …3′ KO Allele 2
B
WT + EV
KO + EV
KO + Spir-1
NS
SeV 6h
SeV 24h
100
100
63
48
35
IB:Myc
IB:Spir-1
IB:p-IRF3
IB:GAPDH

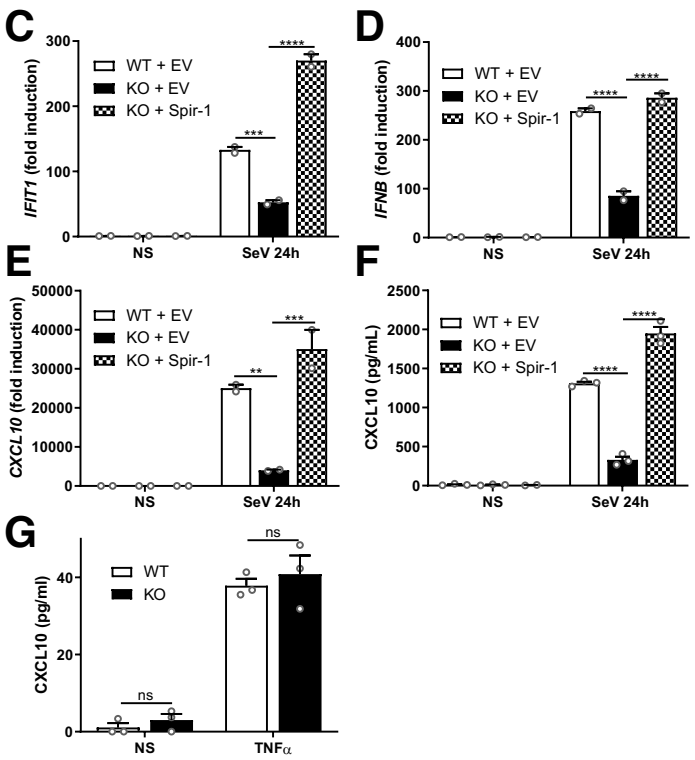
C
IFIT1 (fold induction)
WT + EV
KO + EV
KO + Spir-1
NS
SeV 24h
D
IFNB (fold induction)
E
CXCL10 (fold induction)
F
CXCL10 (pg/mL)
G
CXCL10 (pg/ml)
WT
KO
ns
TNFα

Figure 6

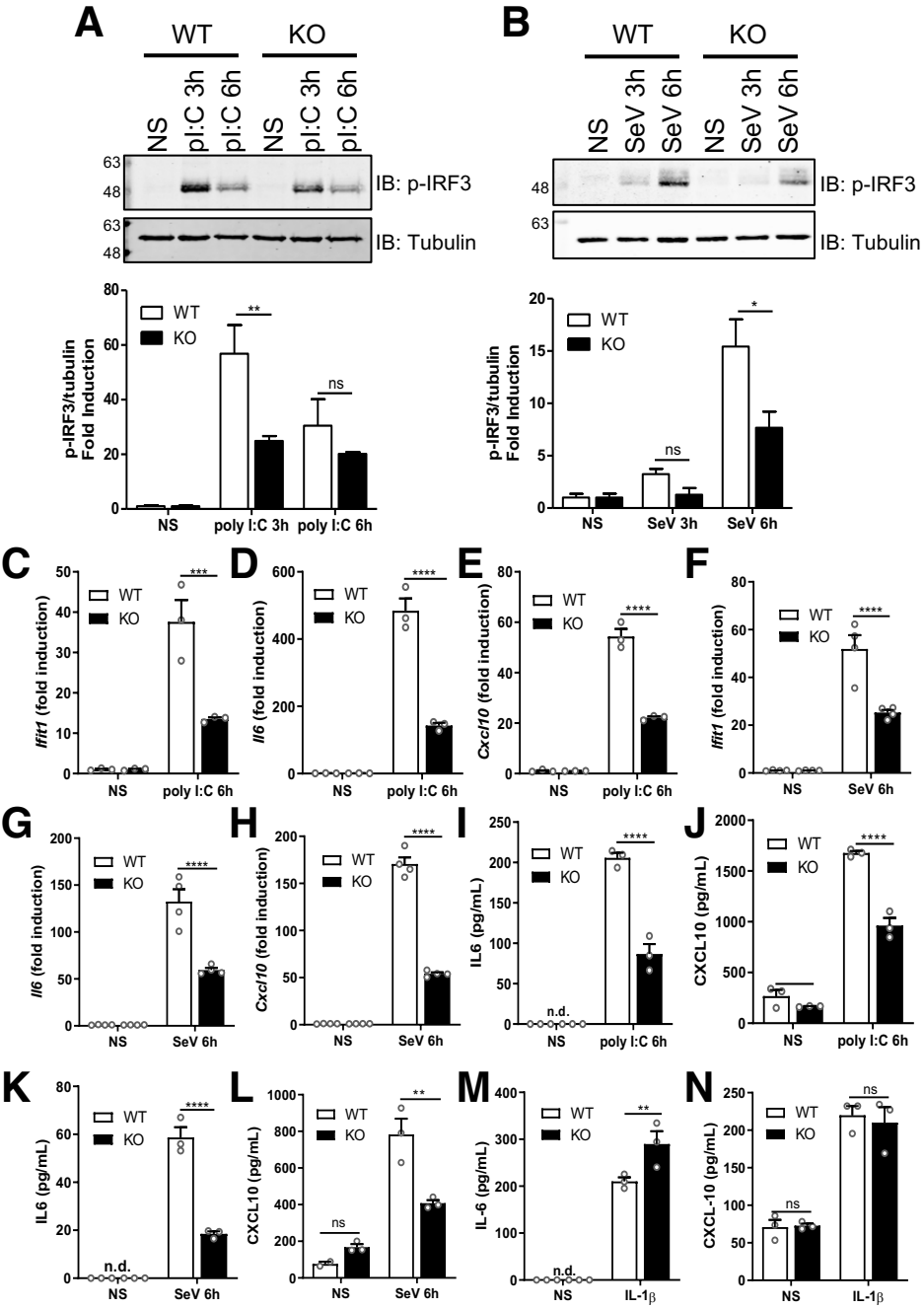
A
WT
KO
NS
pI:C 3h
pI:C 6h
NS
pI:C 3h
pI:C 6h
63
48
IB: p-IRF3
63
48
IB: Tubulin
p-IRF3/tubulin Fold Induction
WT
KO
**
ns
NS
poly I:C 3h
poly I:C 6h
B
WT
KO
NS
SeV 3h
SeV 6h
NS
SeV 3h
SeV 6h
48
IB: p-IRF3
63
IB: Tubulin
p-IRF3/tubulin Fold Induction
WT
KO
*
ns
NS
SeV 3h
SeV 6h
C
Ifit1 (fold induction)
WT
KO
***
NS
poly I:C 6h
D
Il6 (fold induction)
WT
KO
****
NS
poly I:C 6h
E
Cxcl10 (fold induction)
WT
KO
****
NS
poly I:C 6h
F
Ifit1 (fold induction)
WT
KO
****
NS
SeV 6h
G
Il6 (fold induction)
WT
KO
****
NS
SeV 6h
H
Cxcl10 (fold induction)
WT
KO
****
NS
SeV 6h
I
IL6 (pg/mL)
WT
KO
****
n.d.
NS
poly I:C 6h
J
CXCL10 (pg/mL)
WT
KO
****
NS
poly I:C 6h
K
IL6 (pg/mL)
WT
KO
****
n.d.
NS
SeV 6h
L
CXCL10 (pg/mL)
WT
KO
**
ns
NS
SeV 6h
M
IL-6 (pg/mL)
WT
KO
**
n.d.
NS
IL-1β
N
CXCL-10 (pg/mL)
WT
KO
ns
ns
NS
IL-1β

Figure 7

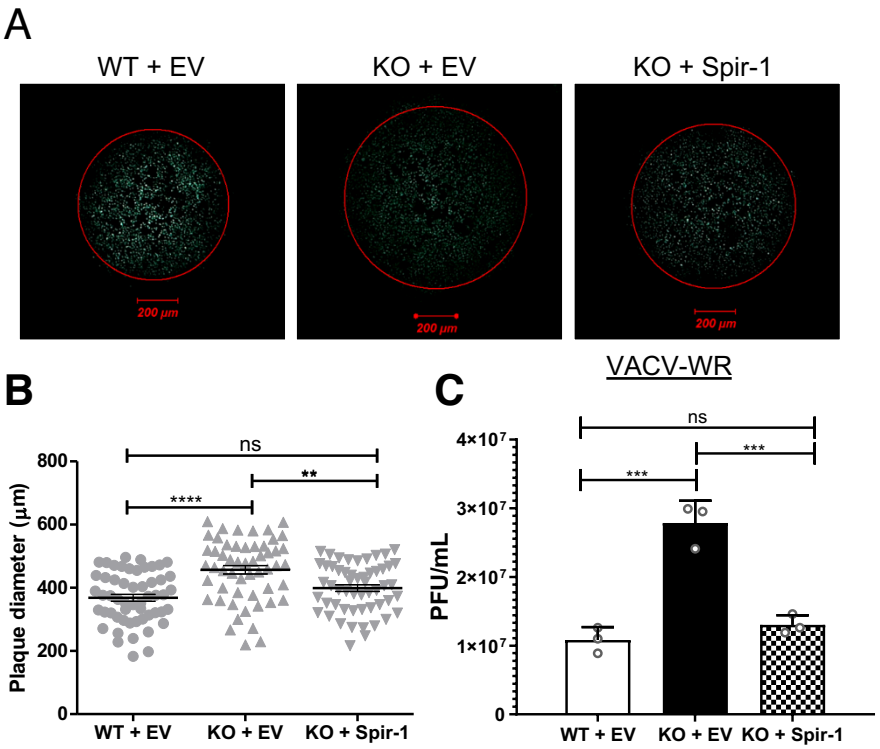
A
WT + EV
KO + EV
KO + Spir-1
200 µm
200 µm
200 µm
B
Plaque diameter (µm)
800
600
400
200
0
ns
****
**
WT + EV
KO + EV
KO + Spir-1
C
VACV-WR
PFU/mL
4×10^7
3×10^7
2×10^7
1×10^7
0
ns
***
***
WT + EV
KO + EV
KO + Spir-1

Figure EV1

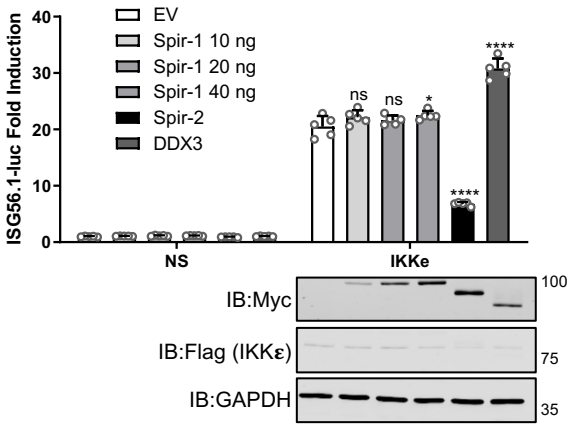
ISG56.1-luc Fold Induction
40
30
20
10
0
EV
Spir-1 10 ng
Spir-1 20 ng
Spir-1 40 ng
Spir-2
DDX3
ns
ns
*
****
****
NS
IKKe
IB:Myc
IB:Flag (IKKε)
IB:GAPDH
100
75
35